Available online at www.sciencedirect.com
SCIENCE DIRECT®
Journal of Solid State Chemistry 178 (2005) 2555–2573
JOURNAL OF SOLID STATE CHEMISTRY
www.elsevier.com/locate/jssc

Functional microporous materials of metal carboxylate: Gas-occlusion properties and catalytic activities

Wasuke Mori*, Tomohiko Sato, Tesushi Ohmura, Chika Nozaki Kato, Tohru Takei

Department of Chemistry, Faculty of Science, Kanagawa University, Hiratsuka, Kanagawa 259-1293, Japan

Received 1 March 2005; received in revised form 16 June 2005; accepted 5 July 2005

Abstract

Copper(II) terephthalate is the first transition metal complex found capable of adsorbing gases. This complex has opened the new field of adsorbent complex chemistry. It is recognized as the lead complex in the construction of microporous complexes. This specific system has been expanded to a systematic series of derivatives of other isomorphous transition metals, molybdenum(II), ruthenium(II, III), and rhodium(II). These complexes with open frameworks are widely recognized as very useful materials for applications to catalysis, separation at molecular level, and gas storage.

Keywords: Gas-occlusion properties; Transition metal carboxylate polymer complex; Self-assembly; Metalloporphyrin; Microporous material; Olefin hydrogenation; Hydrogen exchange reactions

1. Introduction

Microporous inorganic–organic hybrid coordination polymers have attracted much attention because of their gas storage [1–6], ion exchange [7–11], and catalytic properties [12–18]. The synthesis and characterization of infinite one-, two-, and three-dimensional (1D, 2D, and 3D) networks have been an area of rapid growth. When compared with conventional porous materials such as zeolite, activated carbon, porous silica, clay, carbon fabric, etc., these coordination polymers are thought to have future potential. The reason for this is that possibilities exist for designing these coordination polymers for achieving desirable pore shapes and sizes, high porosity, and flexible frameworks, which are governed by the topological properties of the precursor metal ions and ligands.

Previously, we discovered that copper(II) terephthalate [2,13], as shown in Fig. 1, occluded a large amount of gases such as N_2, Ar, O_2, and Xe. Various transition metal dicarboxylates were synthesized as the first step in producing new porous materials. Polydentate ligands are suitable for producing stable covalent networks. (Softness of the structure is required.) The general method for synthesizing a 3D porous complex is shown in Chart 1. The uniform linear micropores in these complexes are constructed by the stacking or bonding of 2D lattices of dinuclear transition metal carboxylates. The intermolecular interactions are more important for producing porous structures consisting of lower-dimensional building blocks. In this study, we selected dinuclear and mononuclear carboxylates as the building blocks.

Recently, we have specifically studied the syntheses and catalytic performances for the heterogeneous hydrogenation catalyses of rhodium carboxylate coordination polymers, e.g., rhodium(II) fumarate ($[Rh_2(trans\text{-}OOCC_2H_2COO)_2]_n$) and rhodium(II) terephthalate ($[Rh_2(p\text{-}OOCC_6H_4COO)_2]_n$), and the rhodium carboxylate polymer complex having a porphyrin ring, e.g., ($[Rh_2(H_2TCPP)]_n$) ($H_2TCPP = 4,4',4'',4'''$-(21*H*,23*H*-porphine-5,10,15,20-tetrayl)tetrakis benzoic acid). Very recently, when tested among some

*Corresponding author. Fax: +81 463 58 9684.
E-mail address: wmori@kanagawa-u.ac.jp (W. Mori).

0022-4596/$ - see front matter © 2005 Elsevier Inc. All rights reserved.
doi:10.1016/j.jssc.2005.07.009

rhodium-containing materials such as rhodium carboxylate coordination polymers rhodium terephthalate, and other reported materials, the rhodium carboxylate polymer complex, $[Rh_2(H_2TCPP)]_n$, was demonstrated to exhibit the highest catalytic activity for the hydrogenation of propene at lower reaction temperatures [13,16,17]. As these studies progressed, we focused chiefly on the syntheses of dinuclear rhodium(II) carboxylates having metalloporphyrin, MTCPP ($M = Cu^{2+}$, Ni^{2+}, and Pd^{2+}), as bimetal hydrogenation catalysts [18].

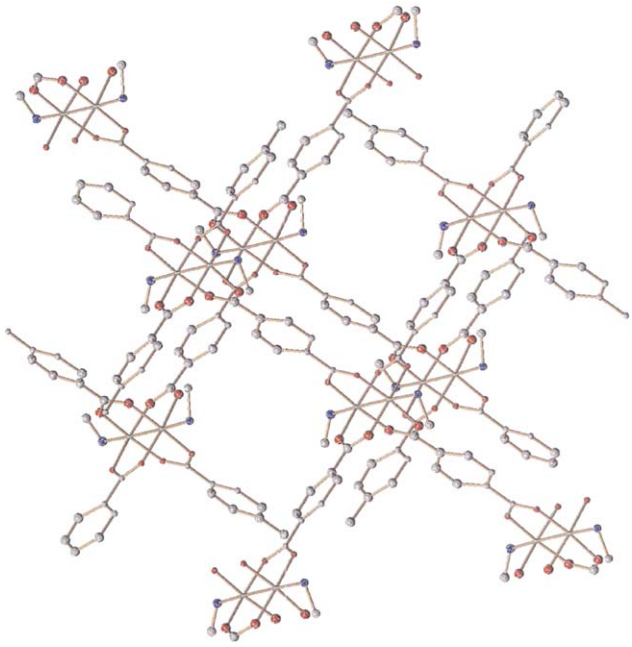

Fig. 1. View of the infinite two-dimensional lattice with micropores of copper(II) terephthalate.

In this paper, we report on the gas storage of novel adsorbent coordination polymers of dinuclear and mononuclear metal(II) dicarboxylates (see Section 2), the catalytic activities of 2D microporous polymers of rhodium(II) dicarboxylates, a novel rhodium(II) carboxylate polymer complex having porphyrin for the hydrogenation of ethene, propene, and 1-butene at 200 K (see Section 3) and, finally, the catalytic performance and bimetallic effects of microporous rhodium(II) carboxylate polymer complexes having metalloporphyrin (see Section 4).

2. Design strategy to synthesize micropore complexes

In 1959, the microporous coordination polymer was reported by Asai et al. [19]. However, there was little interest in such materials until the early 1990s, when

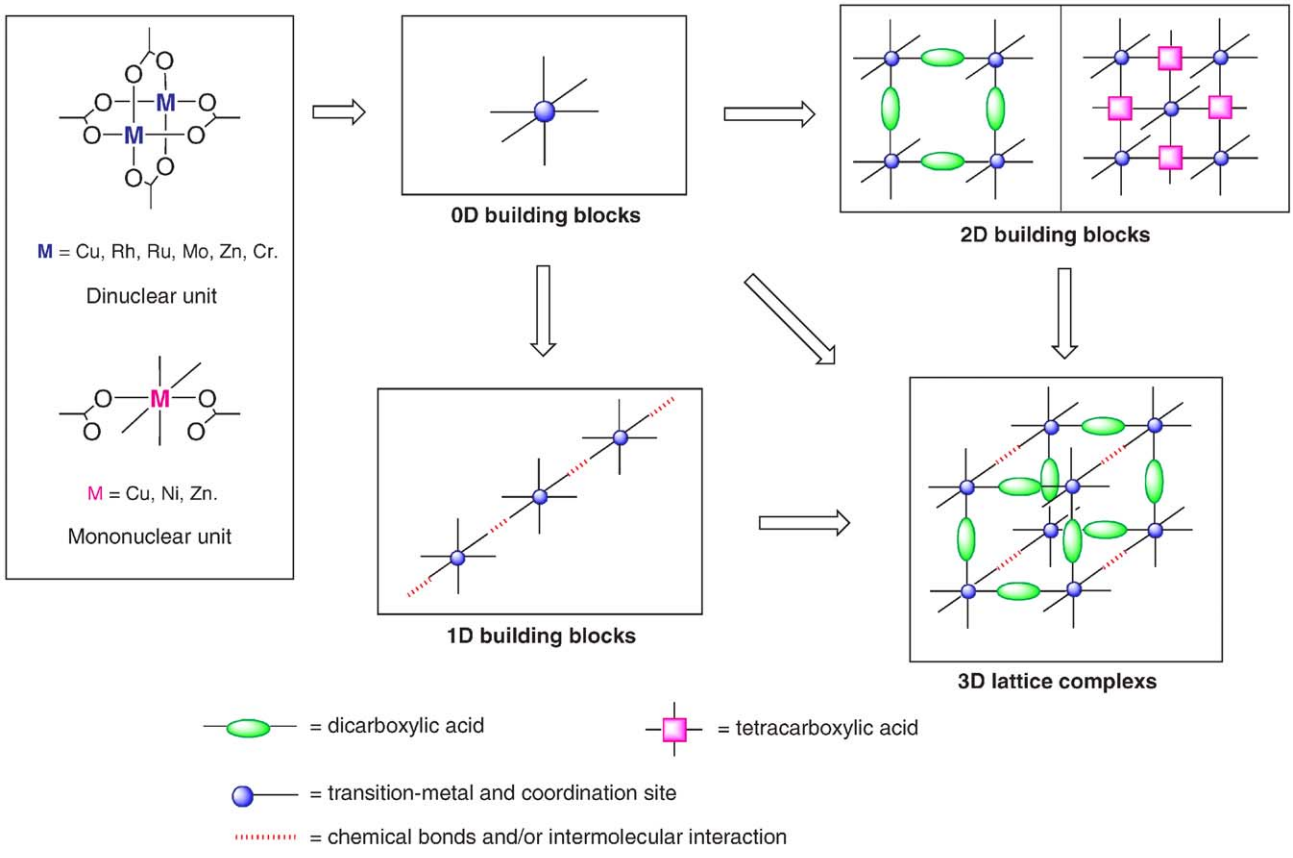

Chart 1. Three-dimensional lattice organized by assembly of low-dimensional building blocks.

Hoskins and Robson [7] reported a porous coordination polymer capable of an anion exchange. Fujita et al. [12] studied the catalytic properties of the 2D coordination polymer in 1994. Since 1995, after we had applied to patent adsorbed microporous complexes [21], we have continued to study adsorbent microporous complexes [13]. In the same year, Moore and co-workers [20] studied the adsorption of guest molecules, in 1997, Kitagawa and co-workers [4] and Mori et al. [2] studied gas adsorption properties under mild conditions (at ambient temperature or pressure), and in 1998, Yaghi and co-workers [1] reported the adsorption of N_2(g) and CO_2(g) for zinc(II) terephthalate.

2.1. Dinuclear transition metal dicarboxylate

Because it was found that copper(II) terephthalate occluded a large amount of gases such as N_2, Ar, O_2, CH_4, and Xe, various transition metal dicarboxylates, $M_2(p\text{-}CH_3C_6H_4COO)_4$ (0D) (M = Cu, Rh, and Mo) [22], $[M_2(C_6H_4COO)_4(pyz)]_n$ (1D) (M = Cu and Rh) [23], $[M_2(OOC\text{-}L\text{-}COO)_2]_n$ (2D) (M = Cu, Mo, Rh, and L = organic ligand) [2,13,16,24], and $[Cu_2(OOC\text{-}L\text{-}COO)_2(TED)]_n$ [25] were synthesized as the first step in producing new porous materials. All complexes reversibly adsorb gases without any structural damage. The surface area, micropore volume, and pore diameter are summarized in Table 1. The pore sizes of metal carboxylates are controllable by the size and structure of carboxylate ligands.

2.1.1. Zero-dimensional building blocks

It was found that special dinuclear transition metal carboxylates such as $M_2(p\text{-}CH_3C_6H_4COO)_4$ (0D) (M = Cu, Rh, and Mo) [22] reversibly adsorbed a large amount of gases. Microcrystals of these complexes, capable of adsorbing gases, were obtained by removal of the guest molecules under vacuum at 373 K. These complexes were linked by guest molecules through weak interactions and uniform capillaries constructed by stacking and self-assembly. The solid-state structure was characterized by single-crystal X-ray crystallography and X-ray powder diffraction (XRPD) measurements. The observed XRPD pattern shows that the porous network was retained in the absence of the included guest molecules.

2.1.2. One-dimensional building blocks

We found the microporous structure to be constructed by self-assembly of infinite linear chain complexes, transition metal benzoates, and substituted benzoate bridged by pyrazine $[M_2(C_6H_4COO)_4(pyz)]_n$ (1D) (M = Cu and Rh) [23]. Their micropores are constructed by the self-assembly (π–π stack) of the component chains, which adopt a perfectly linear geometry with the chain skeleton bridged by the pyrazine group in the axial direction of the dinuclear transition metal benzoate. The values of the BET surface areas of these complexes were equal to that of copper(II) terephthalate.

2.1.3. Two-dimensional building blocks

Generally, a 2D or 3D network structure is built up by bridges of dicarboxylate or polycarboxylate ligands [24]. In the case of the linear dicarboxylate bridges, it is obvious that 2D lattices are constructed, and infinite linear micropores are created by stacking the 2D lattices $[M_2(OOC\text{-}L\text{-}COO)_2]_n$ (2D) (M = Cu, Mo, Rh, and L = organic ligand), as shown in Chart 1. These coordination polymers with open frameworks are widely recognized as very useful materials for applications such as catalysis, separation at the molecular level, and template, supramolecular, and gas storage, as shown in Fig. 2.

2.1.4. Three-dimensional building blocks

We have focused on ruthenium(II, III) dicarboxylate derivatives [25] $[Ru_2^{II,III}(OOC\text{-}L\text{-}COO)_2X]_n$, which construct a more rigid network structure, assisted by axial-halogen bridges, than those of other transition metal dicarboxylates $[M_2(OOC\text{-}L\text{-}COO)_2]_n$ (2D) [24]. These complexes have the ability to adsorb large amounts of

Table 1
Microporosity of coordination polymers obtained by Ar adsorption

Complexes	Dimension	BET surface area ($m^2 g^{-1}$), ($\times 10^3 m^2 mol^{-1}$ of metal)			
		Cu	Rh	Mo	Ru
$M_2(p\text{-}CH_3C_6H_4COO)_4$	0	124 (41.4)	151 (56.4)	159 (58.2)	0
$M_2(C_6H_4COO)_4(pyz)$	1	Not measured	353 (135)	—	36.6 (14.0)
$M_2(trans\text{-}1,4\text{-}OOCC_6H_{10}COO)_2$	2	347 (81.1)	243 (66.4)	213 (56.7)	—
$M_2(trans\text{-}OOCC_2H_2COO)_2$	2	416 (73.9)	325 (70.5)	469 (98.4)	—
$M_2(p\text{-}OOCC_6H_4COO)_2$	2	545 (124)	469 (125)	519 (135)	—
$M_2(trans\text{-}OOCC_2H_2COO)_2(X)$[a]	3	606 (140)	—	—	411 (95.7)
$M_2(p\text{-}OOCC_6H_4COO)_2(X)$[a]	3	1891 (531)	—	—	321 (90.8)

[a] X = triethylenediamine (TED), Cl for copper(II) dicarboxylates, and Ru(II, III) dicarboxylate, respectively.

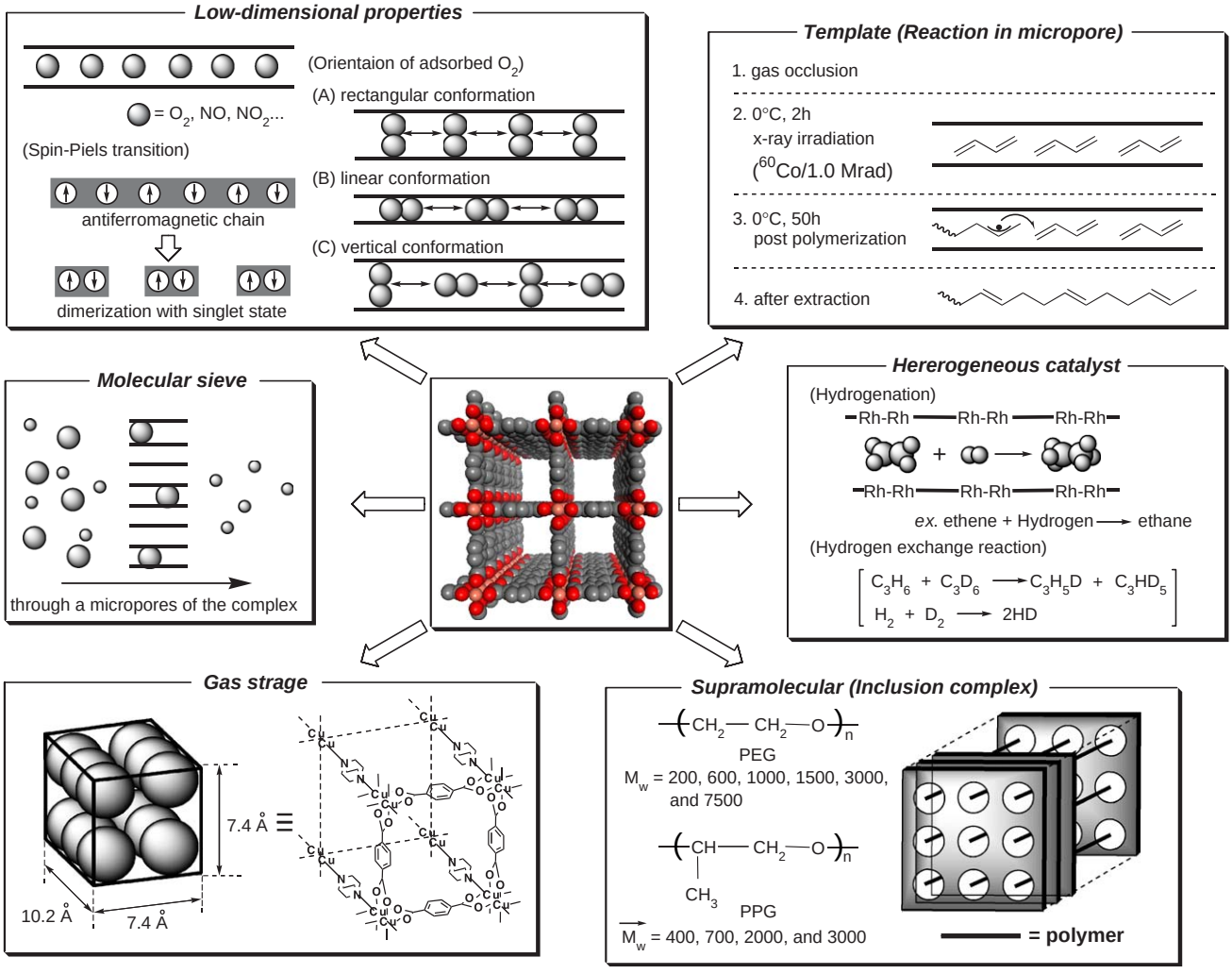

Fig. 2. Applications of microporous complex.

gases, but all complexes reversibly adsorb gases with structural damage. It has been demonstrated that an axial-bridged layer structure is effective for the construction of 3D networks with large channels although this axial-halogen-bridged network has been unstable in the absence of included guest molecules. We have developed a new method for synthesizing stable axial-bridged structures using organic axial ligands. We have also synthesized the porous structure of copper(II) dicarboxylates with triethylenediamine (TED) as the organic axial ligand with copper(II) dicarboxylate derivatives $[Cu_2^{II}(OOC\text{-}L\text{-}COO)_2(TED)]_n$ (L = organic ligand). This structure was maintained at up to 473 K in the absence of the included guest molecules [26].

2.2. Synthesis and structure of metal-organic frameworks with micropores of mononuclear copper(II) carboxylates–pyridine derivatives

Metal-organic framework and polydedra have been widely studied in solution and state for a variety of purposes such as molecular sieve, gas occlusion, and catalyst. There has been recent research interest in crystal engineering supramolecular architectures assembled form metal ions and organic ligands by coordinate covalent bonding, hydrogen bonding, and π-stacking. This is ascribed to a variety of coordination geometries of building blocks.

In this paragraph, we focus interest mainly on coordination polymers with mononuclear metal units instead of dinuclear metal units. Because, the simplicity to obtain the single crystals for the microporous polymer of mononuclear metal carboxylates. Also, the amounts of occluded gas per metal atom of the mononuclear complexes are larger than that of the dinuclear complexes, which the crystalline materials with small amount of metal atoms discovered in this paragraph are advantageous adsorbents for the environment [27].

Chart 2 exhibits the distribution and occurrence of 0D, 1D, and 2D structures. Mononuclear metal(II) monocarboxylates were synthesized using pyridine and

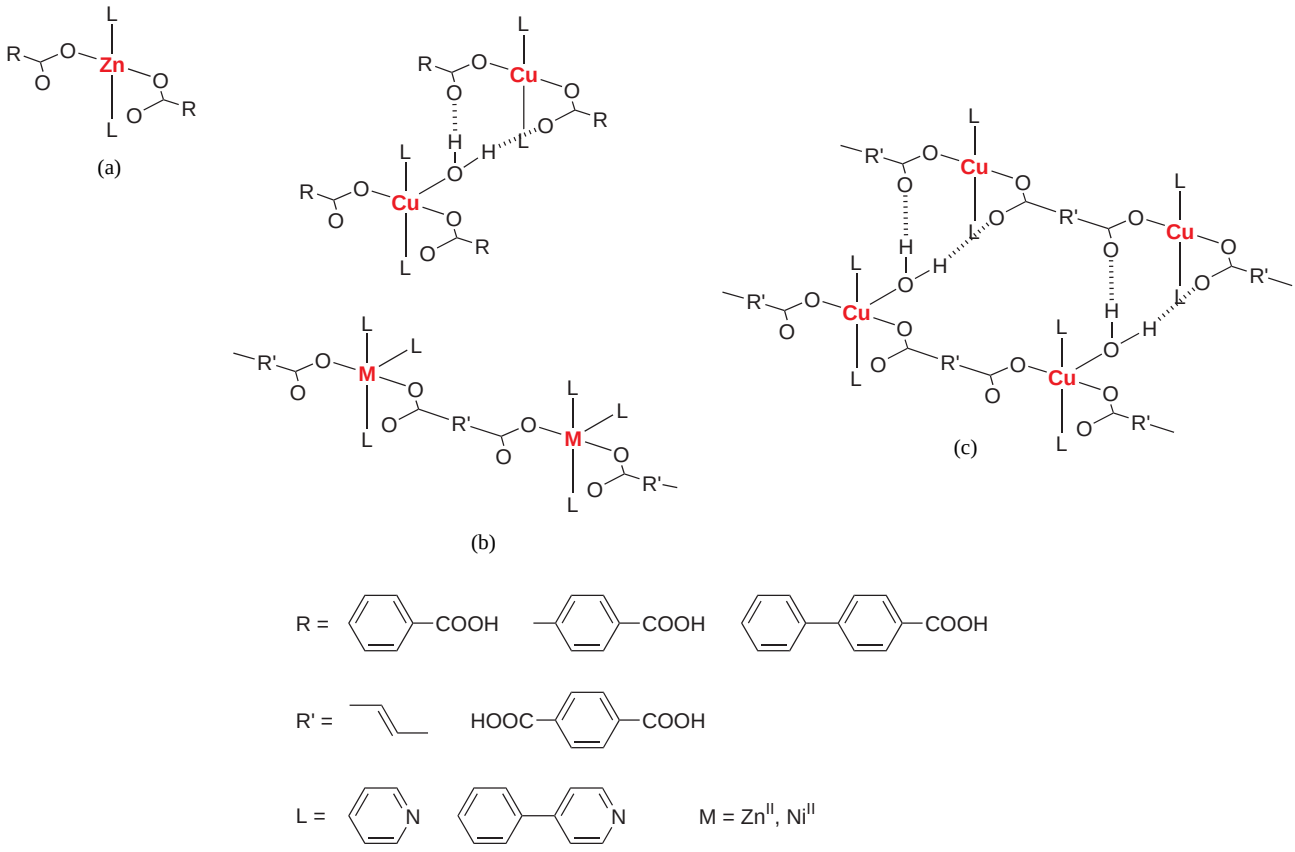

Chart 2. Types of metal-organic frameworks: (a) zero-dimensional structure, (b) one-dimensional structure, and (c) two-dimensional structure.

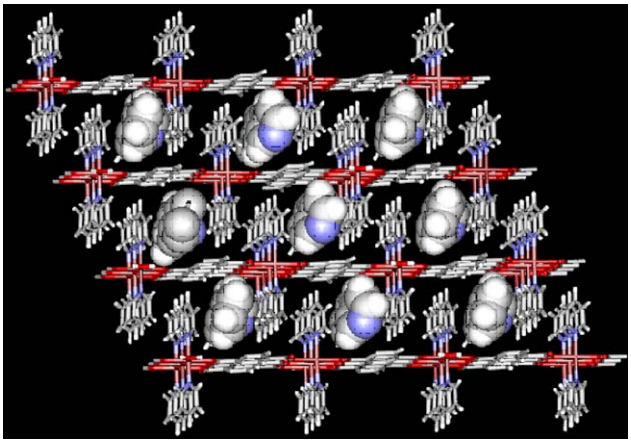

Fig. 3. Structural features of copper(II) terephthalate–pyridine, using a Rigaku/MSC program packages.

p-phenyl pyridine, but have no cavities, and indicate no gas-occlusion properties. Recently, it was found that mononuclear copper(II) terephthalate, which occludes large amounts of gases. Other complexes, mononuclear copper(II) carboxylates, form hydrogen-bonded network, whose micropores occupied guest molecules, after removal guest molecules exhibit gas-occlusion properties [27]. Packing diagram view of copper(II) terephthalate–pyridine including guest molecules are shown in Fig. 3. The channels have an effective diameter of about 4.6 Å. This complex consisting of hydrogen bonding and terephthalate bridging between the Cu(II) ions form 2D structure. In contrast to the metal(II) dicarboxylates, metal(II) monocarboxylates have no cavities, and indicate no gas-occlusion properties.

3. Functions of coordination polymers

3.1. Adsorption properties of copper(II) trans-1,4-cyclohexanedicarboxylate

Copper(II) complexes of fumarate, 2,6-naphthalenedicarboxylate, and *trans*-1,4-cyclohexanedicarboxylate have been prepared as adsorbents. All complexes reversibly adsorb gases without any structural damage. We have investigated gas adsorption properties of copper(II) *trans*-1,4-cyclohexanedicarboxylate, which was not decomposed by moisture and adsorbate. The adsorption isobars of NO, NO_2, CO_2, and SO_2 were measured using a quartz spiral balance in an all-glass system. The complex exhibited the capability of

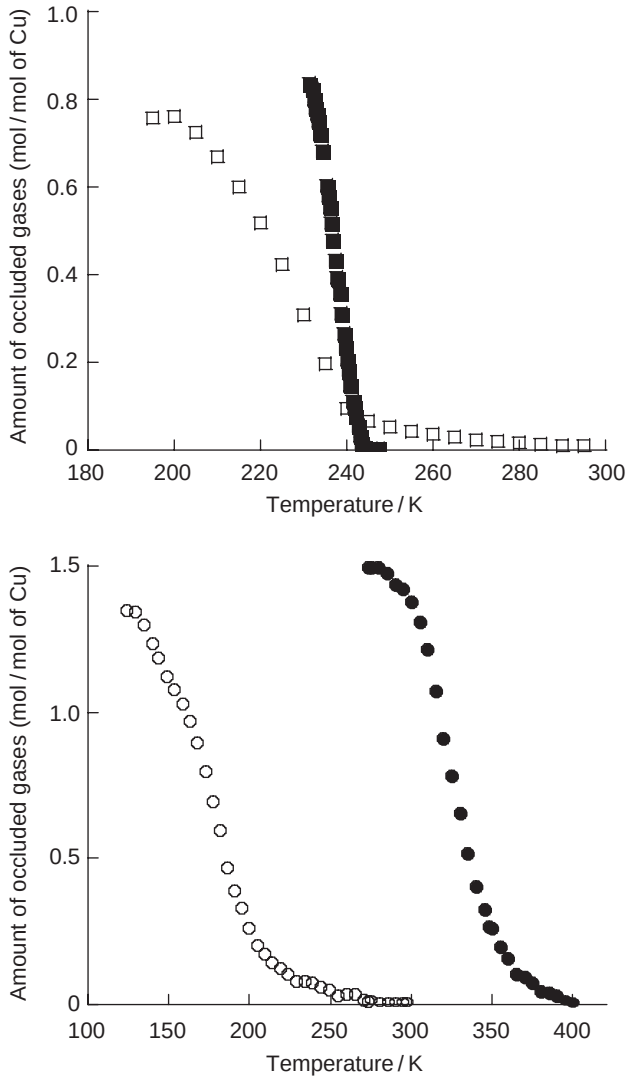

Fig. 4. Adsorption isobars of copper(II) *trans*-1,4-cyclohexanedicarboxylate for CO_2 (□), SO_2 (■), NO (○), and NO_2 (●).

adsorbing gases such as NO, NO_2, CO_2, and SO_2, as shown in Fig. 4. Carbon dioxide was adsorbed into the complexes at temperatures below 300 K, and the maximum amount of adsorbed gas was finally attained around the sublimation temperature (195 K). For the temperature dependence of the amount of adsorbed sulfur dioxide, the gas adsorption behavior was rapid. The maximum amounts of adsorbed CO_2 and SO_2 were 0.76 and 0.84 mol mol^{-1} of copper atoms, respectively. These results indicate that the temperature range of adsorption was influenced by the affinity of the gases for the micropore walls of the copper complex. In contrast, the gas adsorption behavior for the isobar of NO was equal to that of NO_2. The temperature ranges of NO and NO_2 adsorption were different from each other. The maximum amounts of adsorbed nitrogen oxide (NO and NO_2) were 1.5 mol mol^{-1} of copper atoms, which were about two times that of the CO_2 (0.76) and SO_2 (0.84) adsorptions. These results suggest the presence of dimmer species such as $(NO)_2$ and (N_2O_4).

3.2. Catalytic performance for hydrogenation of olefin over rhodium(II) carboxylate

Development of an effective catalytic hydrogenation reaction to preferentially produce the desired materials has been challenged from the viewpoint of both fundamental and industrial applications [28]. Rhodium-containing porous and nonporous materials have received attention in the field of various heterogeneous, hydrogenation catalysts, e.g., organometallic Rh complexes on silica [29] or zeolite [30], diatomic Rh site on carbon [31], immobilization of Rh diphosphine complex on Al-MCM-41 [32], metal oxide deposits on Rh foil [33], molecular-imprinting Rh-dimer on silica surface [34], and polymer-attached Rh complex ($[Rh(NBD)LL]^+$ (L = polyphosphine ligand)) [35]. All these materials are shown to be highly active in the hydrogenation of olefins, carbon dioxide, and carbon monoxide.

The microporous inorganic–organic hybrid coordination polymers have attracted much attention because of their molecular adsorption [1–6], ion-exchange [7–11], and catalytic properties [12–18]. When compared with the conventional porous materials such as zeolite or activated carbons, these coordination polymers are found to have potential for the future. This is because a possibility exists for designing these coordination polymers for achieving the desirable pore shape and size, high porosity, and flexible framework, which are governed by the topological properties of the precursor metal ions and ligands. $[Rh(diisocyanobiphenyl)_2^+ Cl^-]$ is an example of hydrogenation catalyst that uses the inorganic–organic hybrid material [36].

Based on the efficient properties of porous inorganic–organic materials, we have specifically studied the syntheses and catalytic performances for the heterogeneous hydrogenation catalyses of rhodium carboxylate coordination polymers, e.g., rhodium(II) fumarate $[Rh_2(trans\text{-}OOCC_2H_2COO)_2]_n$ (**1**), rhodium(II) terephthalate $[Rh_2(p\text{-}OOCC_6H_4COO)_2]_n$ (**2**), and rhodium(II) 4,4′,4″,4‴-(21*H*,23*H*-porphine-5,10,15,20-tetrayl)tetrakis benzoate $[Rh_2(H_2TCPP)]_n$ (**3**). The uniform linear micropores in these complexes are constructed by the stacking or bonding of 2D lattices of dinuclear transition metal carboxylates. Furthermore, single-site dinuclear transition metal centers in the uniform linear pores are significant characteristics for the use of these metal carboxylates as heterogeneous catalysts. In addition, all the single metal centers can act as active centers during the heterogeneous catalysis. In addition, these complexes are capable of occluding large amounts of gases such as N_2, Ar, O_2, CH_4, and Xe, and show the highest catalytic activities under the conditions

Table 2
Microporosity obtained by Ar adsorption and maximum amount of adsorbed N_2 for complexes **1**–**3**

Complexes		Surface area[a]		Micropore volume ($cm^3\,g^{-1}$)	Pore size (Å)	Amount of adsorbed N_2 ($mol\,mol^{-1}$ of Rh)
		BET	Langmuir			
Rh fumarate	**1**	325 (70)	392 (85)	0.13	5.4	0.87[b]
Rh terephthalates	**2**	469 (125)	596 (212)	0.20	6.0	1.11[b]
$[Rh_2(H_2TCPP)]_n$	**3**	339 (168)	416 (206)	0.14	5.1	2.87[b] (5.74)[c]
H_2TCPP		10.1	13.1	—	—	0.66[c]

[a]$[m^2\,g^{-1}$, $(\times 10^3\,m^2\,mol^{-1}$ of Rh)].
[b]$mol\,mol^{-1}$ of Rh.
[c]$mol\,mol^{-1}$ of porphyrin.

of low temperature and low pressure (30 Torr) during the hydrogenation of ethene, propene, and 1-butene [13,16,17].

In this study, we especially focused on rhodium carboxylate polymer complexes to develop the newer hydrogenation catalysts because the rhodium atom has the interesting properties of chemisorption, dissociation of hydrogen molecules, and hydrogen transfer [37].

In general, modification of the structure of rhodium active centers in heterogeneous catalysts is quite difficult because the structures of rhodium centers are dramatically influenced by the synthetic conditions. For example, rhodium metal catalysts dispersed on polyphosphine supports and rhodium foil with TiO_2 overlayers have shown high catalytic activities for the hydrogenation of ethene, but the relationships between the catalytic activities and the structures of the rhodium centers are still unclear [35,38]. In this section, we specifically report the catalytic performances of rhodium carboxylate polymer complexes **1**–**3** for the heterogeneous hydrogenation of ethene, propene, and 1-butene at 200 K, the unique bimolecular pathway between 2D sheet structures in uniform micropores.

3.2.1. Materials

Rhodium(II) fumarate $[Rh_2(trans\text{-}OOCC_2H_2COO)_2]_n$ (**1**), rhodium(II) terephthalate $[Rh_2(p\text{-}OOCC_6H_4COO)_2]_n$ (**2**), and rhodium(II) 4,4′,4″,4‴-(21*H*,23*H*-porphine-5,10,15,20-tetrayl)tetrakis benzoate $[Rh_2(H_2TCPP)]_n$ (**3**) were synthesized and purified by a published method [13,16,17].

3.2.2. Catalytic hydrogenation of olefins

The hydrogenation reactions and hydrogen exchange reactions of olefins (ethene, propene, and 1-butene) were carried out at 255 and 194 K, respectively. Complexes **1**–**3** were placed into a reaction vessel, which was connected to a conventional closed gas circulation system (350 cm^3). After performing the evacuation at 298 K and H_2 reduction at 373 K for 1 h, the reaction gas comprising 30 Torr olefin and 60 Torr H_2 was introduced. The hydrogenation products were determined by gas chromatography (GC). The reaction product was analyzed by GC (TCD, activated alumina stainless columns) and assignments were made by after comparing these with the authentic samples analyzed under the same conditions.

3.2.3. Synthesis and characterizations of complexes 1–3

Complexes **1**–**3** were synthesized by the ligand-exchange reaction of rhodium(II) acetate with organic ligand. The compositions and structures of complexes **1**–**3** were obtained by the elemental analysis, infrared spectra, TG/DTA, magnetic susceptibilities measurements, XRPD, adsorption isotherms, and pore size distributions. The surface area, micropore volume, and pore diameter are summarized in Table 2. Ar adsorption measurements of complexes **1**–**3** show a sharp pore size distribution at 5.4, 6.0, and 5.1 Å, respectively, and occlude about 0.8, 1.2, and 2.9 $mol\,mol^{-1}$ of Rh atoms, suggesting that these complexes may possess a 2D sheet structure which is constructed of nanoscale micropores with a 3D packing as similar to copper(II) telephthalate, as shown in Fig. 1. Note that nonporous materials do not occlude gases at all. Although complex **3** had smaller pore size, 5.1 Å, than those of complex **1**, and **2**, this complex showed excellent gas-occlusion properties, i.e., the maximum amount of occluded N_2 gas was 2.87 $mol\,mol^{-1}$ of Rh at 77 K, which was about three times that of complex **1**, and **2** at 77 K. The result suggests that the micropores in complex **3** constructed by half metal atoms compared with the complex **1**, and **2**, as shown in Chart 1. Several lines of powder X-ray diffraction patterns for these, though these lines are broad, also suggest that these samples are crystalline materials. Magnetic susceptibilities data also show that these complexes have dinuclear rhodium structures.

3.2.4. Hydrogenation reactions of olefins catalyzed by complexes 1–3

The hydrogenation of olefin (ethene and propene) catalyzed by complexes **1**–**3** was conducted at 194 and 255 K, respectively. The results are summarized in Table 3. The high activities of complexes **1**–**3** necessitate

Table 3
Catalytic activities for hydrogenation of olefins (ethane and propene) and hydrogen exchange reaction of propene catalyzed by complexes **1**–**3**[a]

Catalysts		Reaction temperature (K)	TOF/g[b] [(TOF/Rh)][c]		
			Ethene	Propene (propane formation)	Propene (propene-d_1 formation)
Rh fumarate	**1**	255	5.50×10^{-5} (1.19×10^{-2})	2.40×10^{-5} (5.20×10^{-3})	2.6×10^{-3} (5.64×10^{-1})
		194	1.49×10^{-7} (3.24×10^{-5})	5.02×10^{-8} (1.09×10^{-5})	—
Rh fumarate (dark green)	**1-(B)**	255	—	8.30×10^{-6} (1.80×10^{-3})	(0.0×10^{-3})
Rh fumarate (pale green)	**1-(C)**	255	—	1.20×10^{-5} (2.60×10^{-3})	—
Rh terephthalates	**2**	255	9.70×10^{-5} (2.60×10^{-2})	2.88×10^{-5} (7.70×10^{-3})	—
$[Rh_2(H_2TCPP)]_n$	**3**	194	2.16×10^{-5} (1.07×10^{-2})	6.24×10^{-6} (3.10×10^{-3})	—

[a]Reaction conditions: catalyst, 0.12 mmol; olefin (ethane and propene), 30 Torr; H_2, 60 Torr; and He, 1.4 Torr.
[b]TOF/g = [(mol of product) $g^{-1} s^{-1}$] for hydrogenation hydrogen exchange reactions of olefin at reaction temperatures of 194 and 255 K, respectively.
[c]TOF/Rh = [(mol of product)(atom of Rh)$^{-1}$ g^{-1}] for hydrogenation hydrogen exchange reactions of olefin at reaction temperatures of 194 and 255 K, respectively.

reaction at a low temperature in order to secure a low initial rate. This also leads to and the resulting freedom from complications arising from the influence of mass and heat transport. For ethene hydrogenation, turnover frequency (TOF = [(mol of product) $s^{-1} g^{-1}$]) of complex **3** was 2.16×10^{-5} [(mol of product) $s^{-1} g^{-1}$], which was about 145 times that of complex **1** (1.49×10^{-7}) with 100% selectivity of ethane. For propene hydrogenation, the product was propane with 100% selectivity and the conversion reached up to 15.5% after 360 min. TOF for complex **3** was 6.24×10^{-6}, which was about 124 times that of complex **1** (5.02×10^{-8}). A various rhodium-containing materials, e.g., Rh foil with TiO_2 overlayers [33] and Rh/polyphosphine metal catalyst [35], were used as catalysts for hydrogenation reaction but they required reaction at higher temperature of 323 K. Magnetic susceptibility for complex **3** after pretreatment under hydrogen at 373 K for 1 h showed the same result as that of as-prepared complex **3**, suggesting that the dinuclear rhodium(II) centers in complex **3** were stable active centers under our reaction conditions. These facts suggested that the dinuclear rhodium coordination polymer with porphyrin-containing carboxylate was an effective material for gas adsorption and catalytic hydrogenation of olefin.

As control experiments, the complex **1**-(**b**) having chemical composition was similar to the complex **1**, but did not occlude N_2, maybe due to the incomplete packing of 2D sheets, and complex **1**-(**c**) having very broad (10–20 nm) pore size distributions were used as catalysts for the hydrogenation of olefins. The complexes were put into a reaction vessel, which was connected to a conventional closed gas circulation system. After evacuation at room temperature, complexes **1** and **2** exhibited high catalytic activities for H_2–D_2 exchange reaction even at 200 K. Moreover, the hydrogen exchange of olefins such as ethene, propene, and 1-butene as well as their hydrogenation occurred at 200 K.

Table 3 summarizes the initial rates of propane formation in the C_3H_6–H_2 reaction as well as propene-d_1 formation in the C_3H_6–C_3D_6 reaction over various polymer complexes. It is interesting to note that only the hydrogenation proceeded over the complex **1**-(**b**) but not the hydrogen exchange reaction of the olefin molecules. As previously mentioned, complex **1**-(**b**) did not occlude N_2 due to the incomplete packing of the sheets. This result suggests that the active sites for the hydrogen exchange of the olefins may only exist inside the micropores of the polymer complexes, while hydrogenation of the olefins takes place both inside and at the outer surface of the polymer complexes. In the case of the complex **1**-(**c**) complex, both hydrogenation and the hydrogen exchange reaction of propene took place with rates slower rates than complex **1** and deactivated rapidly after a few times of reported reactions. Recovery to its original activity did not occur even after the 373 K reduction.

Next, to determine the reaction mechanism, we measured the deuterium isotopic distribution by microwave spectroscopy. Microwave spectroscopy is an excellent technique for the study of hydrogen exchange or isomerization reaction of propene or 1-butene [39], because it enables us to determine the distribution of the D atoms in the exchanged d_1-molecules. Fig. 5a shows microwave spectroscopic analyses of the deuterium isotopic distribution of formed propene-d_1 during C_3H_6–C_3D_6 reaction over the complex **1** at 194 K, where *cis*- and *trans*-propene-1-d_1 were the main products and the amounts of propene-2-d_1 and 3-d_1 were very small. In contrast, the exchange rate of the C_3H_6–D_2 reaction was two orders of magnitudes smaller than that of the C_3H_6–C_3D_6 reaction. Fig. 5b shows the isotopic distribution pattern of this reaction, which was

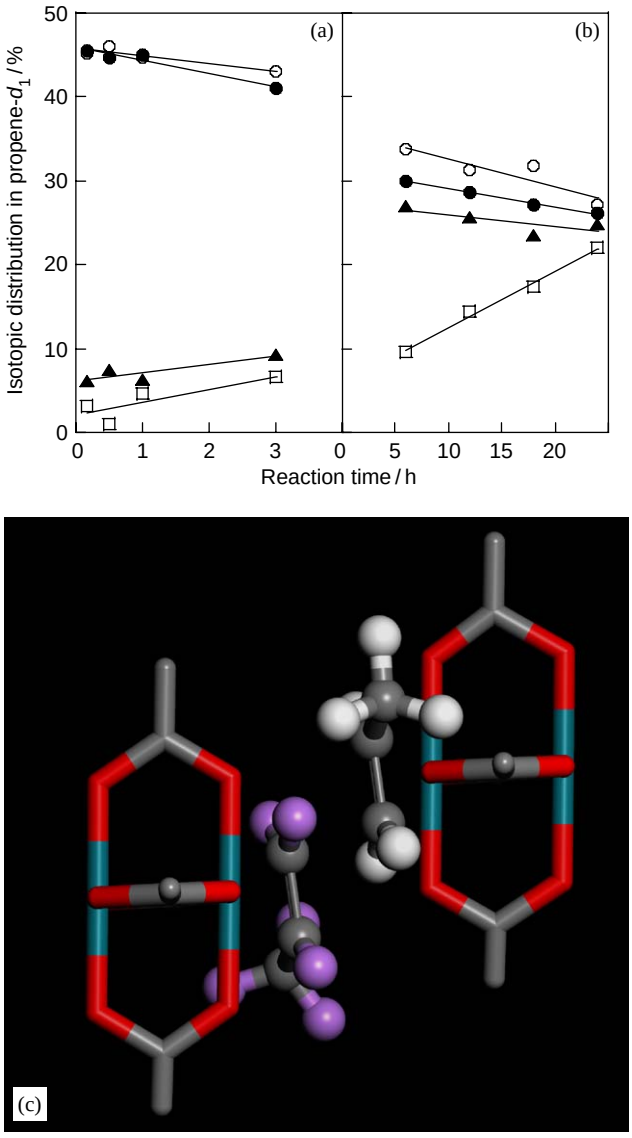

Fig. 5. Time course of (a) C_3H_6–C_3D_6 and (b) C_3H_6–D_2 reactions over complex **1** at 194 K, and (c) schematic drawing of an intermediate of a four-centered carbon ring structure formed by two propene molecules in the bimolecular pathway.

different from that of the C_3H_6–C_3D_6 reaction, and operation of the 1,3- and 2,3-intramolecular hydrogen exchange processes [39]. To study the relationship between adsorbed hydrogen and propene, the initial rates of HD formation in the H_2–D_2 and C_3H_6–H_2–D_2 reactions, and also initial rates of propene-d_1 formation in the C_3H_6–C_3–D_6 and C_3H_6–C_3D_6–H_2 reactions, were compared over the complex **1** at 194 K. The initial rates of HD formation in the H_2–D_2 and C_3H_6–H_2–D_2 reactions were comparable, and one order of magnitude faster than that of propene-d_1 formation in the C_3H_6–C_3D_6 reaction. In contrast, the initial rate of propene-d_1 formation in the C_3H_6–C_3D_6–H_2 reaction was identical to that of the C_3H_6–C_3D_6 reaction with the same isotopic distribution. These results indicate that

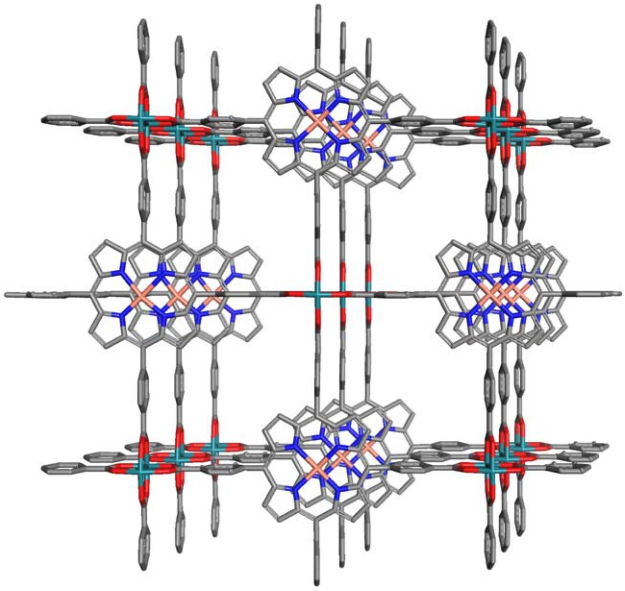

Fig. 6. Deduced molecular structure of $[Rh_2(MTCPP)]_n$ ($M = H_2$ **3**, Cu^{2+} **4**, Ni^{2+} **5**, and Pd^{2+} **6**). Elements are color-coded: rhodium (green), carbon (gray), nitrogen (blue), oxygen (red), and M (pink).

intermolecular hydrogen exchange between two propene molecules takes place independently of the dissociative adsorption of hydrogen molecules.

As previously discussed, the C_3H_6–C_3D_6 exchange reaction only occurs inside the micropores of the complexes. The direct dissociative mechanism of the propene C–H bond is not available for this exchange process because no mixing was observed between the hydrogen of the propene molecules and the dissociative hydrogen of the gaseous hydrogen molecules. Accordingly, we propose the following mechanism for this exchange process. When two propene molecules are put into the channel of the three-dimensionally packed sheets, they might exchange their hydrogen without complete scission of the C–H bond. Microwave spectroscopic analysis of propene-d_1 formed in this reaction indicates that only the hydrogen atoms attached to the double bond carbons of propene are exchangeable and suggests the existence of an intermediate of a four-centered carbon ring structure formed by two propene molecules, as shown in Fig. 5c. Naito and co-workers have already reported the existence of such a novel exchange mechanism, which does not involve a complete C–H bond dissociation but rather an intermolecular hydrogen shift between two adsorbed propene molecules over alumina-supported $Os_3(CO)_{12}$ derived catalysts. Co-existing adsorbed CO modifies the electronic state of the Os and makes the direct dissociation mechanism unfavorable, opening a new bimolecular pathway [40]. In the present study, a special electronic micropore structure as well as restricted nanospace may play an important role for the operation of such a novel reaction

pathway. With regard to the reaction mechanism of complex **3**, the kinetic parameters, activation energies (E_a; 42.0 kJ mol^{-1}), activation enthalpies ($\Delta^{\ddagger}H$; 39.9 kJ mol^{-1}), and activation entropies ($\Delta^{\ddagger}S$; -517 J K^{-1} mol^{-1}), calculated on the basis of the reaction rates for hydrogenation reactions of propene catalyzed by complex **1**, and **3** in the temperature range of 194–255 K also provided efficient aspects for the consideration of the reaction mechanism. The E_a value of complex **3** was similar to that of complex **1** (41.6 kJ mol^{-1}), suggesting that the reaction mechanism at the rhodium center of complex **3** was the same as that of complex **1**. Furthermore, the activation entropies for complexes **1** and **3** were -518 and -517 J K^{-1} mol^{-1}, respectively, which were significantly smaller than that of Rh dimer-imprinted SiO_2 (-276 to -170 J K^{-1} mol^{-1}) [34], suggesting that the conformation of the coordinated propene was highly regulated by the micropore walls of complex **1**, and **3**.

4. Development of more efficient catalysts

The synthesis of multimetallic active centers at molecular levels is one of the significant technologies utilized in developing more efficient hydrogenation catalysts [41]. Several supported multimetal catalysts have been extensively studied for their role in various heterogeneous reactions, and the roles of multimetallic centers have also been investigated. A few examples of rhodium-containing multimetal catalysts are as follows: $[Co_2Rh_2]\cdot(CO)_{12}/SiO_2$ for skeletal rearrangement of hydrocarbon [42]; Cu-*M*/NaY (*M* = Pt, Ir, Rh, and Ru) [43], Ni-*M*/NaY (*M* = Ru, Rh, Pd, and Pt) [44], and Pd–Rh/Al_2O_3 [45] for hydrogenation of the carbon–carbon multiple bond; $[H_2RhOs_3(CO)_{10}(acac)]$/$Al_2O_3$ [46], Rh-Fe/NaY [47], and *M*-Fe^{3+} (*M* = Rh, Pt, and Pd)/SiO_2 [40c] for CO hydrogenation, Ni–Rh/ZrO_2 [48] for CO_2 reforming, and Cu/Rh(100) catalysis for CO oxidation [49]. In some of the multimetallic catalysts, e.g., Ru–Pd/Al_2O_3 [50] and Pt on alkali-borosilicate [51], a hydrogen spillover behavior has been observed, which can accelerate the catalytic reactions significantly [52]. However, the studies on the heterogeneous catalytic activities involving a single active site of the multimetal catalysts are particularly challenging, given the inherent difficulties encountered in characterizing the active sites under the reaction conditions because of the difficulties in synthesizing the active and selective catalytic centers at molecular levels in heterogeneous catalysis [34].

In this study, we have focused on dinuclear rhodium(II) carboxylates $[Rh_2(MTCPP)]_n$ (*M* = H_2 **1**, Cu^{2+} **2**, Ni^{2+} **3**, and Pd^{2+} **4**, as shown in Fig. 6), having metalloporphyrin as bimetal hydrogenation catalysts. In this section, we specifically report the catalytic performances of $[Rh_2(MTCPP)]_n$ for the heterogeneous hydrogenation of ethene, propene, and 1-butene at low temperatures from 194 to 255 K, the unique bimetallic effects between metal centers of porphyrin rings, and the bridged dinuclear rhodium sites in uniform micropores.

4.1. Materials

$[Rh_2(MTCPP)]_n$ (*M* = H_2 **3**, Cu^{2+} **4**, Ni^{2+} **5**, and Pd^{2+} **6**) was synthesized and purified by a published method [18].

4.2. Catalytic hydrogenation of olefins

The hydrogenation reactions of olefins (ethene, propene, and 1-butene) were carried out at 194, 220, and 255 K, respectively. Complexes **3–6** were placed into a reaction vessel, which was connected to a conventional closed gas circulation system (155.7 cm^3). After performing the evacuation at 298 K, the reaction gas comprising 30 Torr olefin and 60 Torr H_2 was introduced. The hydrogenation products were determined by GC. The reaction product was analyzed by GC (TCD, Porapak Q and activated alumina stainless columns), and assignments were made by after comparing these with the authentic samples analyzed under the same conditions.

4.2.1. Synthesis and characterizations of complexes 3–6

$[Rh_2(MTCPP)]_n$ (*M* = H_2 **3**, Cu^{2+} **4**, Ni^{2+} **5**, and Pd^{2+} **6**) were synthesized by the ligand-exchange reaction of rhodium(II) acetate with MTCPP prepared from commercially available H_2TCPP and a metal chloride ($CuCl_2$, $NiCl_2\cdot 6H_2O$, and $PdCl_2$), as shown in Scheme 1. The purity and composition of each of the starting MTCPP were obtained by the elemental analysis, DR–UV–vis spectra, and ^{1}H NMR measurements. The perfect insertion of metal atoms into the center of the porphyrin ring of **3** was impossible. The compositions and structures of complexes **3–6** were obtained by the elemental analysis, infrared spectra, TG/DTA, ^{1}H NMR, DR–UV–vis spectra, magnetic susceptibilities measurements, XRPD, adsorption isotherms, and pore size distributions [18].

To examine the porosity of complexes **3–6**, high-resolution adsorption isotherms of argon at 87.3 K were measured under a relative pressure (P/P_0) range from 10^{-5} to 1. These adsorption isotherms of all complexes show typical isotherms of Langmuir type, confirming the presence of micropores without mesopores. A sharp rise in argon adsorption at low relative pressures ($P/P_0 \leqslant 0.2$) indicated that the micropores are extremely uniform. Analyses of these isotherms yielded BET surface areas, micropore volumes, and effective pore size for all complexes shown in Table 4. In complexes **3–6**, one sharp peak was obtained at 5.1, 5.1, 5.0, and 5.0 Å, respectively, indicating that the obtained com-

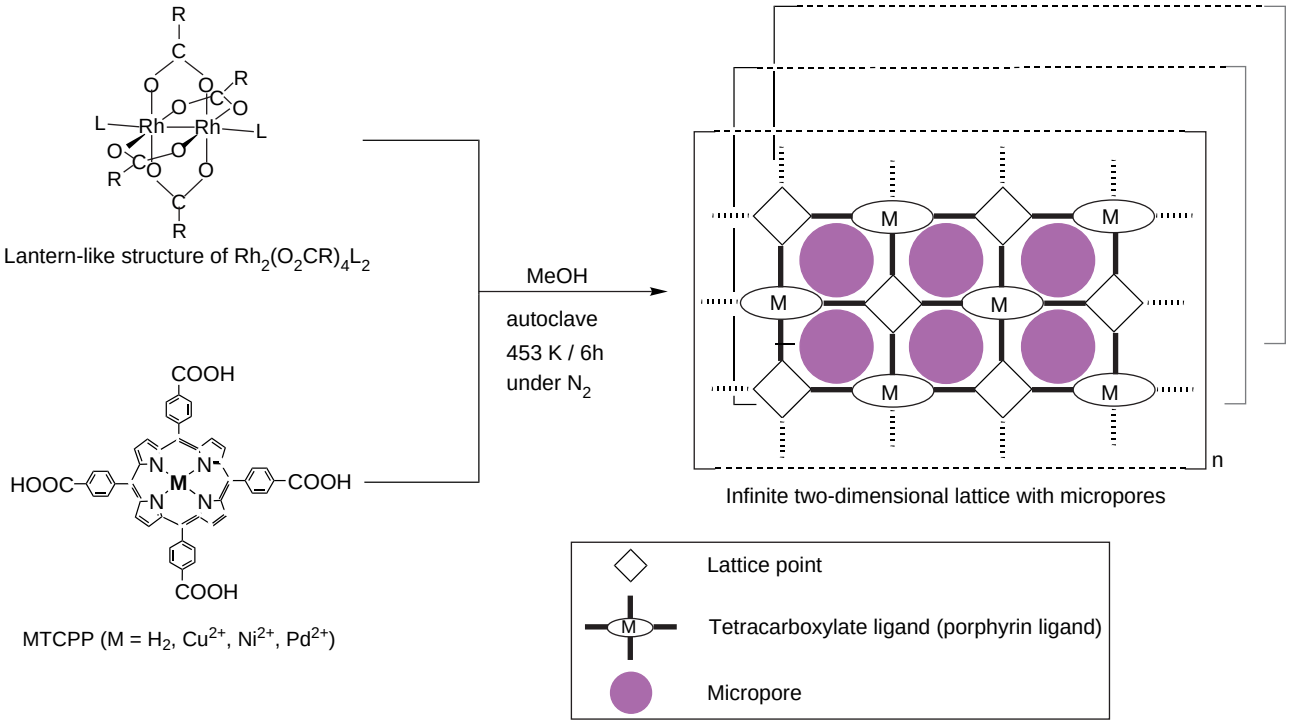

Scheme 1. Synthetic scheme for $[Rh_2(MTCPP)]_n$ ($M = H_2$ **3**, Cu^{2+} **4**, Ni^{2+} **5**, and Pd^{2+} **6**).

Table 4
Microporosity obtained by Ar adsorption and maximum amount of adsorbed N_2 for complexes **3–6**

Complexes		Surface area[a]		Micropore volume ($cm^3\,g^{-1}$)	Pore size (Å)	Amount of adsorbed N_2 ($mol\,mol^{-1}$ of Rh)
		BET	Langmuir			
$[Rh_2(H_2TCPP)]_n$	**3**	339 (168)	416 (206)	0.14	5.1	2.9 (5.7)[b]
$[Rh_2(Cu^{2+}TCPP)]_n$	**4**	373 (197)	456 (241)	0.16	5.1	3.2 (6.4)[b]
$[Rh_2(Ni^{2+}TCPP)]_n$	**5**	299 (157)	361 (190)	0.12	5.0	2.4 (4.7)[b]
$[Rh_2(Pd^{2+}TCPP)]_n$	**6**	318 (174)	387 (212)	0.13	5.0	2.5 (5.0)[b]

[a] $[m^2\,g^{-1}$, ($\times 10^3\,m^2\,mol^{-1}$ of Rh)].
[b] $mol\,mol^{-1}$ of porphyrin.

plexes have uniform micropores. The large surface areas ($299–373\,m^2\,g^{-1}$) and the high micropore porosities ($0.12–0.16\,cm^3\,g^{-1}$) in the area of inorganic–organic hybrid coordination polymers were due to the stacking of 2D $[Rh_2(MTCPP)]_n$ layers as well as other carboxylate coordination polymers [6]. XRPD data of complexes **3–6** also support this result.

To observe the ability of complexes **3–6**, the adsorption isobars ($P = 20$ Torr) of nitrogen in the temperature range of 77.5–200 K were measured. Nitrogen was adsorbed into the complexes at temperatures below 200 K, and the amount of adsorbed gas finally attained the maximum around the boiling temperature of nitrogen. All the complexes were capable of adsorbing a large amount of nitrogen, though amorphous H_2TCPP hardly adsorbed nitrogen ($<0.66\,mol\,mol^{-1}$ of porphyrin). The maximum amounts of nitrogen adsorbed in complexes **3–6**, which were evaluated from the saturated amounts with isobars, were 2.9, 3.2, 2.4, and $2.5\,mol\,mol^{-1}$ of rhodium(II) atoms, respectively, as summarized in Table 4. These absorbed amounts of nitrogen were approximately 2.1–3.7 times larger than those of rhodium(II) fumarate $[Rh_2(trans\text{-}OOCC_2H_2COO)_2]_n$ and rhodium(II) terephthalate $[Rh_2(p\text{-}OOCC_6H_4COO)_2]_n$ [6], and the order of maximum amount (**4** > **3** > **6** > **5**) was in good agreement with that of BET surface area.

4.2.2. Hydrogenation reactions of olefins catalyzed by complexes 3–6

The hydrogenations of olefin (ethene, propene, and 1-butene) catalyzed by complexes **3–6** were conducted at 194, 220, and 255 K, respectively. The results are summarized in Tables 5 and 6. The high activities of

Table 5
Catalytic activities for hydrogenation of propene catalyzed by complexes **3**–**6**[a]

Catalysts		TOF/g[b] [(TOF/Rh)][c]		
		At 194 K	At 220 K	At 255 K
$[Rh_2(H_2TCPP)]_n$	**3**	6.24×10^{-6} (3.10×10^{-3})	3.28×10^{-4} (0.16)	3.17×10^{-3} (1.57)
$[Rh_2(Cu^{2+}TCPP)]_n$	**4**	8.77×10^{-5} (4.62×10^{-2})	1.95×10^{-3} (1.03)	1.02×10^{-2} (5.39)
$[Rh_2(Ni^{2+}TCPP)]_n$	**5**	3.32×10^{-5} (17.4×10^{-2})	5.50×10^{-4} (0.29)	1.21×10^{-2} (6.36)
$[Rh_2(Pd^{2+}TCPP)]_n$	**6**	2.25×10^{-4} (1.24×10^{-1})	2.28×10^{-3} (1.25)	1.35×10^{-2} (7.38)

[a]Reaction conditions: catalyst, 10 mg; propene, 30 Torr; H_2, 60 Torr; and He, 1.4 Torr.
[b]TOF/g = [(mol of product) g^{-1} s^{-1}] for hydrogenation of propene after 180, 15, and 5 min at reaction temperatures of 194, 220, and 255 K, respectively.
[c]TOF/Rh = [(mol of product)(atom of Rh)$^{-1}$ g^{-1}] for hydrogenation of propene after 180, 15, and 5 min at reaction temperatures of 194, 220, and 255 K, respectively.

Table 6
Catalytic activities for hydrogenation of 1-butene catalyzed by complexes **3**–**6**[a]

Catalysts		TOF/g[b] [(TOF/Rh)][c]	
		At 220 K	At 255 K
$[Rh_2(H_2TCPP)]_n$	**3**	2.13×10^{-4} (0.11)	4.62×10^{-4} (0.23)
$[Rh_2(Cu^{2+}TCPP)]_n$	**4**	1.42×10^{-3} (0.75)	7.12×10^{-3} (3.54)
$[Rh_2(Ni^{2+}TCPP)]_n$	**5**	2.44×10^{-3} (1.28)	5.43×10^{-3} (2.70)
$[Rh_2(Pd^{2+}TCPP)]_n$	**6**	4.21×10^{-3} (2.31)	9.17×10^{-3} (4.57)

[a]Reaction conditions: catalyst, 10 mg; propene, 30 Torr; H_2, 60 Torr.
[b]TOF/g = [(mol of product) g^{-1} s^{-1}] for hydrogenation of 1-butene after 15 and 5 min at reaction temperatures of 220 and 255 K, respectively.
[c]TOF/Rh = [(mol of product)(atom of Rh)$^{-1}$ g^{-1}] for hydrogenation of 1-butene after 15 and 5 min at reaction temperatures of 220 and 255 K, respectively.

complexes **3**–**6** necessitate reaction at a low temperature in order to secure a low initial rate. This also leads to and the resulting freedom from complications arising from the influence of mass and heat transport. With regard to the hydrogenation of ethene, the reaction rates were extremely fast to observe even at 194 K.

For obtaining the time course of propene, hydrogenation at 194, 220, and 255 K (Figs. 7a–c), the high catalytic activities of complexes **3**–**6** were observed. Propane with 100% selectivity at all reaction temperatures was obtained as the product. At 194 K, an induction period of <30 min was observed for complexes **3**–**6** because of the physisorption of the produced propane in the micropores. After 180 min, the conversions of complexes **3**–**6** attained 2.7, 47.1, 14.5, and 100%, respectively, showing that complex **6** was the most active, and their turnover frequencies (TOF = [(mol of product) s^{-1} g^{-1}]) were 6.24×10^{-6}, 8.77×10^{-5}, 3.32×10^{-5}, and 2.25×10^{-4}, respectively, showing that the TOF of **6** was 2.6–36 times higher than that of complexes **3**–**5**; and the order of the activity of these complexes for propene hydrogenation was $Pd^{2+} > Cu^{2+} > Ni^{2+} \gg H_2$. At 220 K, the TOFs [(mol of product) g^{-1} s^{-1}] of complexes **3**–**6** were 3.28×10^{-4}, 1.95×10^{-3}, 5.50×10^{-4}, and 2.28×10^{-3} after 15 min, respectively. At 255 K, the conversions of all catalysts attained 100% within 30 min. In particular, the reaction catalyzed by **6** finished within 5 min. The TOFs [(mol of product) g^{-1} s^{-1}] of **3**–**6** were 3.17×10^{-3}, 1.02×10^{-2}, 1.21×10^{-2}, and 1.35×10^{-2} after 5 min, respectively. The catalytic results at 220 and 255 K also showed that complex **6** was the most active complex, and the order of the activity was the same ($Pd^{2+} > Cu^{2+} > Ni^{2+} > H_2$). In addition, these bimetallic effects of Cu–Rh, Ni–Rh, and Pd–Rh were not dependent on the BET surface area, rather they were dependent on the type of metal atoms centered in the porphyrin ring, as shown in Fig. 8. The 100% conversion after 5 min at 255 K and TOF of 1.35×10^{-2} [(mol of product) g^{-1} s^{-1}] (= 7.38 [(mol of product)(atom of Rh)$^{-1}$]) were observed for **6** and compared with those reported for other rhodium(II)-containing systems; the conversion of propene hydrogenation over $[Rh(NBD)(PolyPPh_2)_2]ClO_4$ [35] at 361 K could not exceed 50% even after 7200 min. The TOF values of 9.80×10^{-4} [(mol of product)(atom of Rh)$^{-1}$] for $Cp_2Ta(CH_2)_2Rh(CO)_2$ observed at 318 K and 1.85×10^{-3} [(mol of product)(atom of Rh)$^{-1}$] for $Cp_2Ta(CH_2)_2Rh(CO)(PPh_3)$ observed at 318 K [31] were much lower (10^{-4} times) than that of **6**, respectively. Metal supported catalysts such as Pt/SiO_2 (0.37 mol atom^{-1} of Pt at 220 K) and Pd/SiO_2 (1.6 mol atom^{-1} of Pd at 201 K) [52] showed activities similar to that of **6**, but they required a higher reaction pressure (7.6×10^2 Torr).

The complexes **3**–**6** were also observed to catalyze the hydrogenation of 1-butene to butane (100% selectivity) at 220 and 255 K, as shown in Fig. 9 and Table 6. At 194 K, the reproducibility of measurements was not obtained due to the solidification of 1-butene. At 220 K, an induction period was observed for these complexes due to the physisorption of the produced butane. The conversions of complexes **3**–**6** attained 100% within 60 min. The TOFs [(mol of product) g^{-1} s^{-1}] of **3**–**6** were 2.13×10^{-4}, 1.42×10^{-3}, 2.44×10^{-3}, and 4.21×10^{-3},

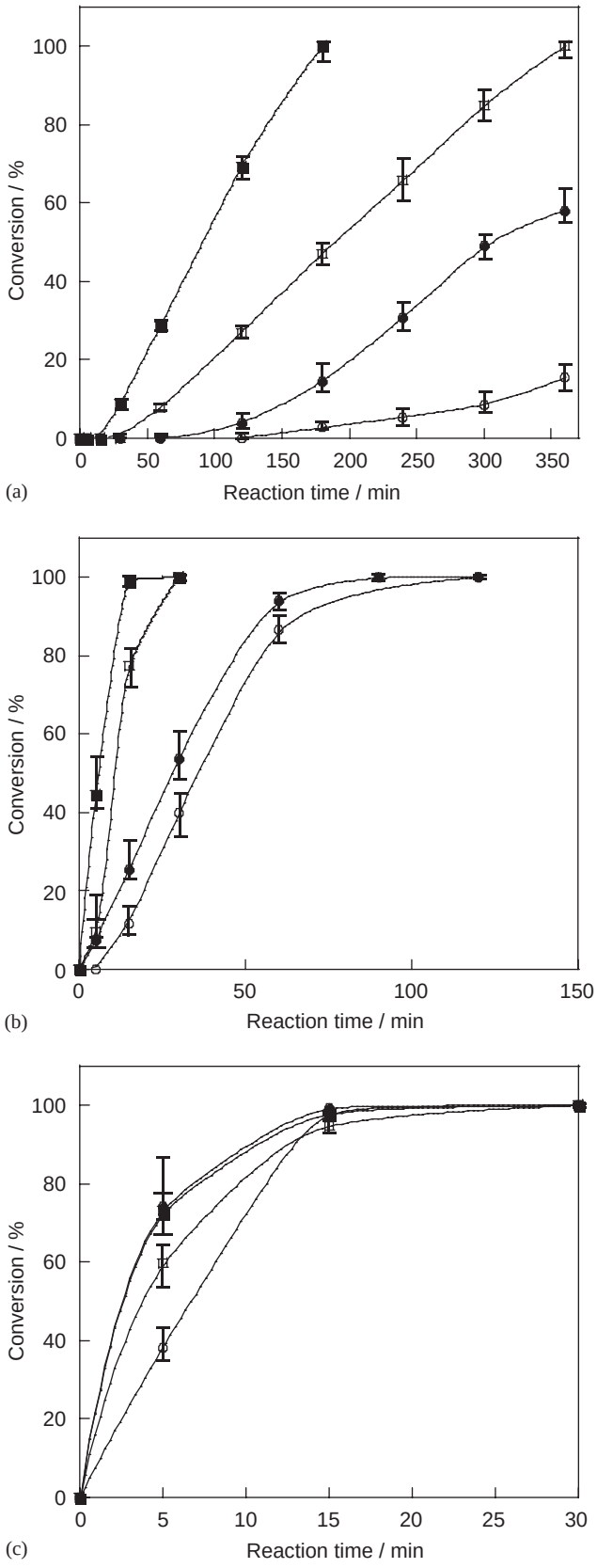

Fig. 7. Time course for hydrogenation of propene catalyzed by $[Rh_2(MTCPP)]_n$ $M = H_2$ (○), Cu^{2+} (□), Ni^{2+} (●), Pd^{2+} (■) at (a) 194 K, (b) 220 K, and (c) 255 K. Reaction conditions: catalyst, 5 and 10 mg; propene, 30 Torr; H_2, 60 Torr.

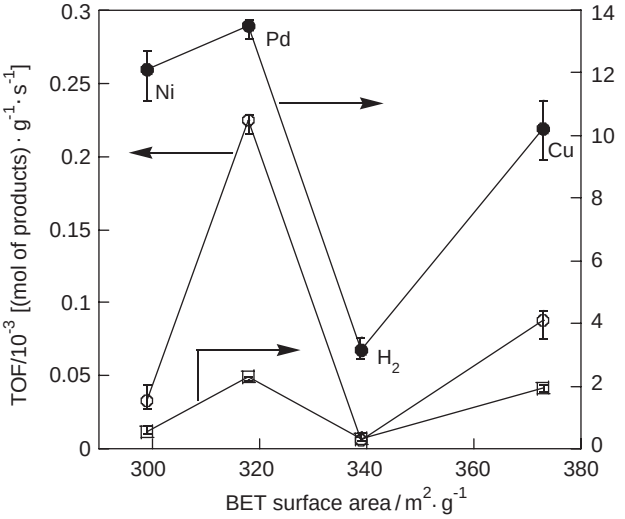

Fig. 8. Surface area dependence of TOFs for propene hydrogenation catalyzed by $[Rh_2(MTCPP)]_n$ ($M = H_2$ **1**, Cu^{2+} **2**, Ni^{2+} **3**, and Pd^{2+} **4**) at 194 K (○), 220 K (□), and 255 K (●).

respectively, suggesting that complex **6** was the most active, and the order of the activity of these complexes for 1-butene hydrogenation at 220 K was $Pd^{2+} > Cu^{2+} \approx Ni^{2+} \gg H_2$. At 255 K, the conversion attained 100% within 30 min. The highest TOF of complex **6** was 9.17×10^{-3}, and the value of TOF was 19.8, 1.3, and 1.7 times those of complexes **3**–**5**, and the same order of activity ($Pd^{2+} > Cu^{2+} > Ni^{2+} > H_2$) was observed for these complexes for hydrogenation of 1-butene. The observed TOF compares favorably with those reported for other heterogeneous systems involving supported metals. For example, $Cp_2Ta(CH_2)_2Rh(CO)_2$ having a TOF of 1.39×10^{-4} [(mol of product)(atom of Rh)$^{-1}$] has been reported to catalyze the hydrogenation of 1-butene. This TOF was much lower than that of **6** 9.17×10^{-3} [(mol of product)(atom of Rh)$^{-1}$] at 255 K. In addition, the TOFs for this reaction have been reported for metal supported catalysts such as Pt/Al_2O_3 (0.85 wt%) at 300 K (TOF: 12) (20 MPa) [52] and $Rh(C_5H_7O_2)_3/\gamma\text{-}Al_2O_3$ (0.23 wt%) at 300 K (TOF: 23.1) (20 MPa) [29d], which had higher activities than that of complex **6**; however, they required conditions of high temperature (300 K) and high pressure (2.6×10^2 Torr).

As control experiments, the 1:1 (mol mol^{-1}) mixtures of $Rh_2(CH_3COO)_4 \cdot 2H_2O$ and MTCPP were used as catalysts for the hydrogenation of propene at 194 K, as shown in Fig. 10. No reaction was observed for any of the catalysts used. Despite the remarkable bimetallic effects observed for the hydrogenation catalysis mentioned above, the 1:1 (mol mol^{-1}) mixtures of $[Rh_2(H_2TCPP)]_n$ and MTCPP ($M = Cu^{2+}$, Ni^{2+}, and Pd^{2+}) also showed lower activities (10^{-1} times) than those of complexes **4**–**6** for the hydrogenation of propene at 194 K, as shown in Fig. 10. In addition, no

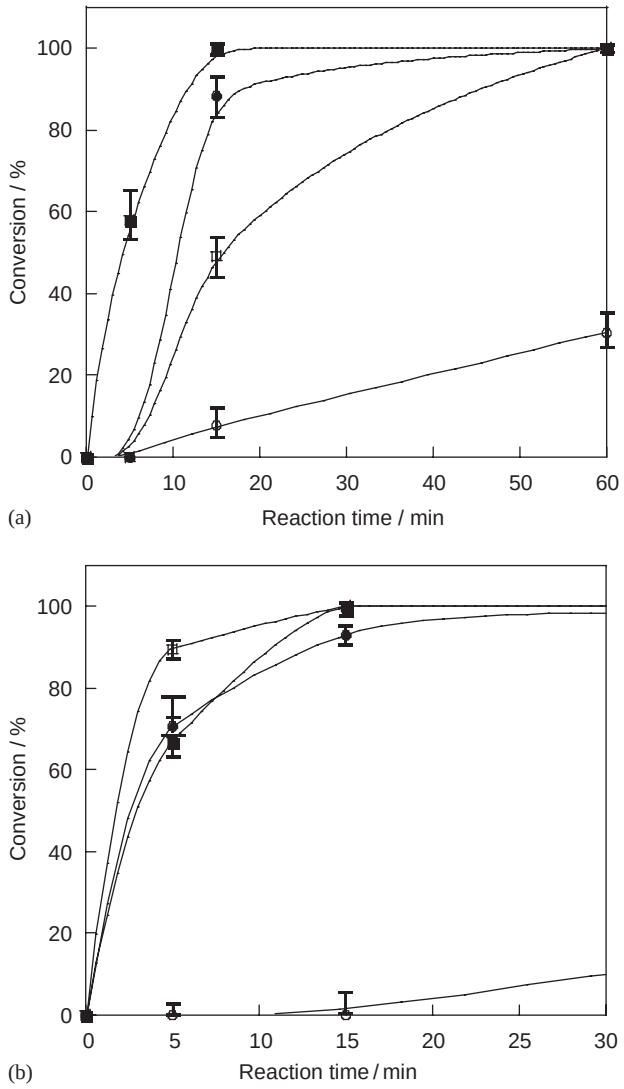

Fig. 9. Time course for hydrogenation of 1-butene catalyzed by $[Rh_2(MTCPP)]_n$ $M = H_2$ (○), Cu^{2+} (□), Ni^{2+} (●), Pd^{2+} (■) (a) at 220 K and (b) 255 K. Reaction conditions: catalyst, 10 mg; propene, 30 Torr; H_2, 60 Torr.

nonporous rhodium carboxylate polymer complex showed any reaction for the hydrogenation reaction of propene at 194 K. These results indicate that (1) the hydrogenation reactions requires Rh centers, (2) the intramolecular distances between the metal atoms centered in the porphyrin ring and the Rh centers are critical for the hydrogenation reactions, and (3) the hydrogenation reaction occurs in the micropores.

4.2.3. Reaction mechanism including bimetallic effects of Rh^{2+}–Cu^{2+}, Rh^{2+}–Ni^{2+}, and Rh^{2+}–Pd^{2+} combinations

To understand the reaction mechanism including the bimetallic effect, the individual roles of the metal atoms centered in the porphyrin ring and the bridged dinuclear rhodium sites for the hydrogenation reactions were investigated. With regard to the hydrogenation reaction

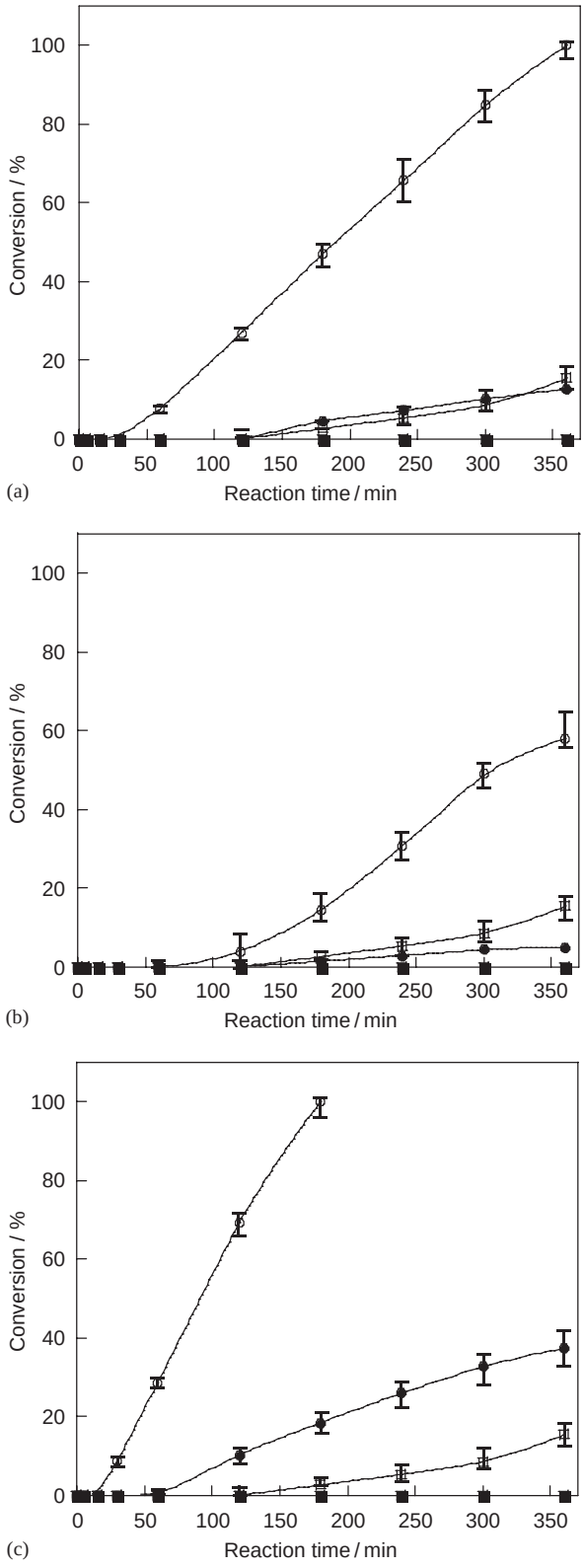

Fig. 10. Time course for hydrogenation of propene at 194 K catalyzed by $[Rh_2(MTCPP)]_n$ (○), $[Rh_2(H_2TCPP)]_n$ (□), the mixture of $[Rh_2(H_2TCPP)]_n + MCl_2$ (●), and the mixture of $Rh_2(CH_3COO)_4 \cdot 2H_2O$ + MTCPP (■). M = (a) Cu^{2+}; (b) Ni^{2+}; (c) Pd^{2+}. Reaction conditions: catalyst, 10 mg; propene, 30 Torr; H_2, 60 Torr.

Table 7
Activation energies (E_a), activation enthalpies ($\Delta^{\ddagger}H$), and activation entropies ($\Delta^{\ddagger}S$) for the catalytic hydrogenation of propene at 255 K

Catalysts		Kinetic parameters		
		E_a (kJ mol^{-1})	$\Delta^{\ddagger}H$ (kJ mol^{-1})	$\Delta^{\ddagger}S$ (J K^{-1} mol^{-1})
Rh fumarate	**1**	41.6	39.5	–518
$[Rh_2(H_2TCPP)]_n$	**3**	42.0	39.9	–517
$[Rh_2(Cu^{2+}TCPP)]_n$	**4**	32.0	29.9	–556
$[Rh_2(Ni^{2+}TCPP)]_n$	**5**	39.8	37.7	–525
$[Rh_2(Pd^{2+}TCPP)]_n$	**6**	27.6	25.4	–573

of olefins that use rhodium-containing catalysts, the well-known hydrogenation mechanism involves four steps [53]: dissociation of hydrogen molecules located at the metal center to form hydrides, coordination of an olefin C=C double bond to the metal center, insertion into the Rh–H bond to form a half-hydrogenated alkyl species, and reaction of the alkyl with the remaining hydride. Based on our previous report regarding the H–D exchange reactions over the microporous rhodium(II) fumarate and rhodium(II) terephthalate [13,16], these typical steps involved in the hydrogenation reaction occurred between the 2D $[Rh_2(trans\text{-}OOCC_2H_2COO)_2]_n$ layers and $[Rh_2(p\text{-}OOCC_6H_4COO)_2]_n$ layers. With regard to the reaction mechanism of complexes **3**–**6**, the kinetic parameters, activation energies (E_a), activation enthalpies ($\Delta^{\ddagger}H$), and activation entropies ($\Delta^{\ddagger}S$) (Table 7), calculated on the basis of the reaction rates for hydrogenation reactions of propene catalyzed by rhodium(II) fumarate and complexes **3**–**6** in the temperature range of 194–255 K also provided efficient aspects for the consideration of the reaction mechanism; the activation energies for complexes **3**–**6** were 42.0, 32.0, 39.8, and 27.6 kJ mol^{-1}, respectively. The E_a value of complex **3** was similar to that of rhodium fumarate (41.6 kJ mol^{-1}), suggesting that the reaction mechanism at the rhodium center of **3** was the same as that of rhodium fumarate. In addition, the E_a values decreased in the order of **3**>**5**>**4**>**6** with the catalytic activities decreasing in the order of **6**>**4**>**5**>**3** for the hydrogenation of propene and 1-butene, suggesting that the metal atoms centered in the porphyrin ring remarkably influenced the activations of hydrogen molecules and/or olefin molecules. Furthermore, the activation entropies for rhodium fumarate and complexes **3**–**6** were −518, −517, −556, −525, and −573 J K^{-1} mol^{-1}, respectively, which were significantly smaller than that of Rh dimer-imprinted SiO_2 (−276 to −170 J K^{-1} mol^{-1}) [34], suggesting that the conformation of the coordinated propene was highly regulated by the micropore walls of rhodium fumarate and complexes **3**–**6**.

Furthermore, to investigate the roles of Cu^{2+}, Ni^{2+}, and Pd^{2+} atoms centered in the porphyrin ring, the hydrogen and propene absorption–desorption measurements were performed at 77.4 and 273.2 K, respectively, as shown in Fig. 11. The saturated amounts of the adsorbed hydrogen at ca. 720 mmHg for complexes **3**–**6** were 76.3, 74.2, 59.6, and 57.4 cm^3 STP g^{-1}, respectively. In the desorption curves of hydrogen, the amounts of hydrogen desorbed were approximately the same as those of adsorbed hydrogen, indicating that very fast, reversible adsorption–desorption of hydrogen occurred in all the complexes. Slight differences were observed for the adsorption–desorption behaviors among complexes **3**–**6**, suggesting that the activation of hydrogen was not influenced by the metal atoms centered in the porphyrin ring. The activation of hydrogen molecule at the bridged rhodium centers was much faster than that of the reported Rh_2 centers at the SiO_2 surface, on which the presence of rhodium hydride species could be detected even at room temperature [34]. The result suggests that the hydride species could not be detected by magnetic susceptibility measurements after pretreatment under a hydrogen atmosphere of 20 Torr at 25 °C for 3 h. The unstable rhodium hydride species were formed at the rhodium centers of complexes **3**–**6**.

In contrast, the saturated amounts of adsorbed propene at ca. 650 mmHg were 59.3, 70.8, 40.3, and 54.8 cm^3 STP g^{-1}, respectively. Hystereses were observed in all the desorption curves of propene. These desorption curves were different from the adsorption ones, showing that the pysisorption of olefin molecules in micropores of complexes **3**–**6** was much stronger than that of hydrogen. The ratios of the residual amounts of propene molecules after desorption to the saturated amounts of adsorbed propene molecules at ca. 40 mmHg were 17.6, 16.0, 28.5, and 14.3, respectively, and the residual amounts were decreased in the order of **6**<**4**<**5**, which was consistent with the reverse order of catalytic activities as mentioned above. Thus, a smooth reversibility of adsorption–desorption of olefin molecules led to higher catalytic activities for the hydrogenation reaction. These results suggest that the metal atoms centered in the porphyrin ring significantly reflect the coordination of the olefin molecules.

Finally, we proposed the reaction mechanism for $[Rh_2(MTCPP)]_n$. In the reactions of $[Rh_2(H_2TCPP)]_n$, the first step included both the addition of hydrogen to

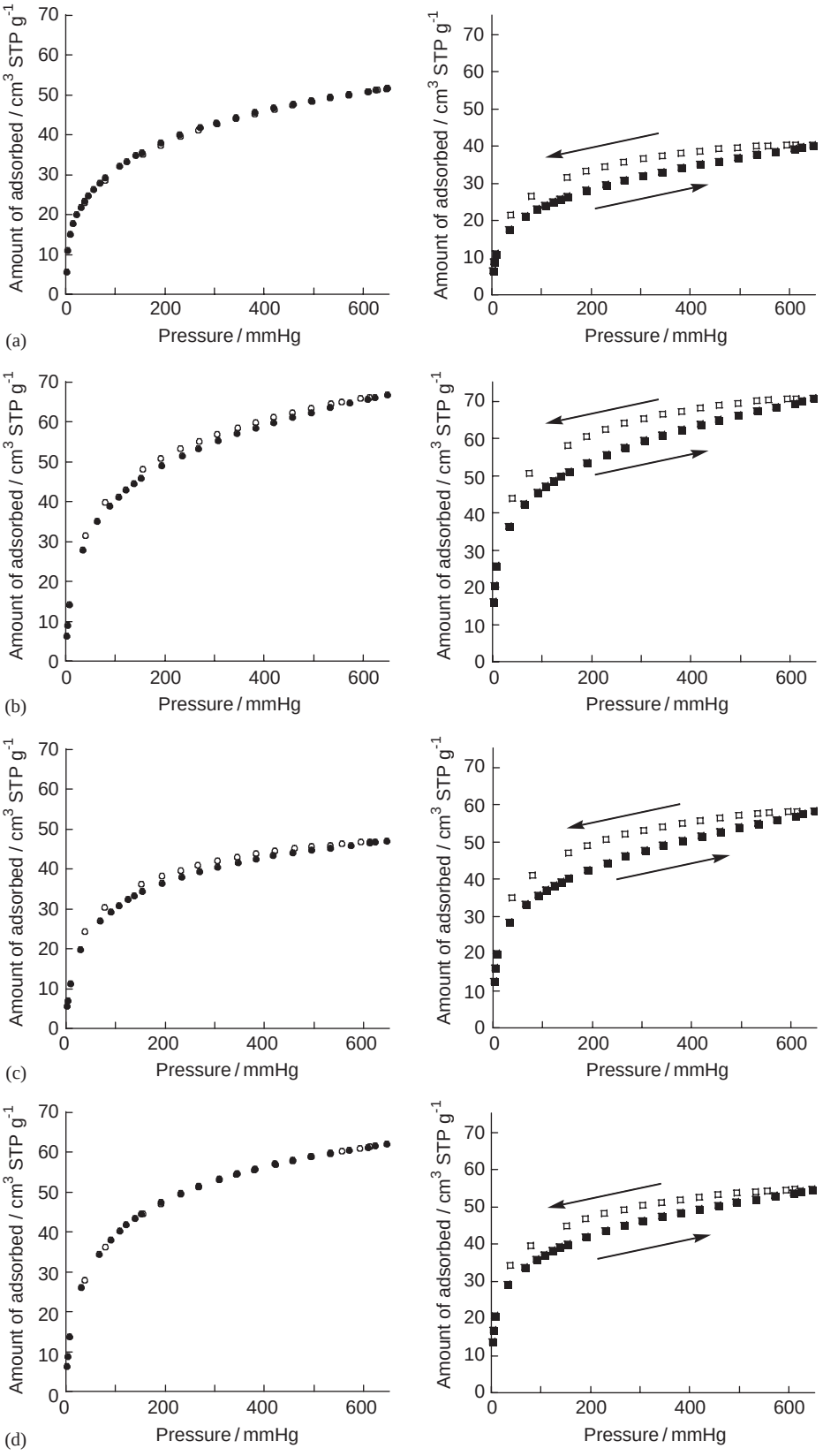

Fig. 11. Adsorption (black)–desorption (white) isotherms of hydrogen at 77.4 K (circle) and propene at 273.2 K (square) for $[Rh_2(MTCPP)]_n$ (M = (a) H_2, (b) Cu^{2+}, (c) Ni^{2+}, (d) Pd^{2+}).

the rhodium center to form hydrides and the coordination of olefins. With regards to complexes **4**–**6**, the priority coordination of olefin onto the metal center of the porphyrin ring also occurred. At the dinuclear rhodium sites, insertion to the Rh–H bond to form a half-hydrogenated alkyl species and the reaction of an alkyl with a hydride occurred continuously. At the Cu^{2+}, Ni^{2+}, and Pd^{2+} centers of the porphyrin ring, the hydride species at the rhodium center got transferred to the coordinated olefin located the center of the porphyrin ring to form alkyl species, and then the alkyl species reacted with a hydride species activated at the rhodium center to form the alkane. This intramolecular hydrogen transfer might significantly influence the catalytic activities during hydrogenation. To our knowledge, this hydrogen transfer was the first example of catalytic behavior using inorganic–organic hybrid materials, though such a hydrogen transfer (hydrogen spillover) has already been observed in the multimetallic oxides and multimetallic clusters [50,51].

5. Conclusion

In the present work, we have succeeded in synthesizing of mononuclear metal(II) monocarboxylates and dicarboxylates, to investigate their crystal structures and magnetic behaviors. Copper(II) complexes, which are self-assembled by hydrogen bonding and π-stacking of phenyl group of mononuclear units, form porous structures. Utilizing the pyridine as a solution simplified to obtain the single crystals for mononuclear metal(II) carboxylates. In comparison with industrially important adsorbents, the system discovered in the present work is the simplest and most advantageous adsorbent for studying pure and applied chemistry, because we apply to the mononuclear copper(II) carboxylates–pyridine derivatives can be converted into special absorbent, exhibit larger amounts of gas-occlusion properties with bidentate axial ligand exchange.

Two-dimensional microporous polymers of Rh fumarate (**1**), Rh terephthalate (**2**), the rhodium carboxylate polymer complex having a porphyrin ring, $[Rh_2(H_2TCPP)]_n$ (H_2TCPP = 4, 4′,4″,4‴-(21*H*,23*H*-porphine-5,10,15,20-tetrayl)tetrakis benzoic acid) complexes (**3**) have exhibited high catalytic activities for hydrogen exchange and hydrogenation of olefins (ethene, propene, and 1-butene) at 200 K. The turnover frequencies of complexes **1**–**3** for hydrogenation of ethene at 194 K are much higher than those of other published Rh-containing materials. The microwave spectroscopic analyses of the deuterium isotopic distribution of formed propene-d_1 during C_3H_6–C_3D_6 reaction over complexes **1** and **2** reveal that the hydrogen exchange reactions take place only inside the nanopores of complexes **1** and **2** without complete scission of C–H bond of olefin molecule. Such a novel bimolecular pathway may play an important role for development of new heterogeneous hydrogenation catalysts.

The novel microporous rhodium(II) carboxylate polymer complexes having metalloporphyrin, $[Rh_2(MTCPP)]_n$ ($M = H_2$ **3**, Cu^{2+} **4**, Ni^{2+} **5**, and Pd^{2+} **6**) (H_2TCPP = 4,4′,4″,4‴-(21*H*,23*H*-porphine-5,10,15,20-tetrayl)tetrakis benzoic acid), were synthesized by the ligand-exchange reactions of rhodium acetate with MTCPP. These were completely characterized by elemental analysis, TG/DTA, magnetic susceptibility, FT-IR, DR–UV–vis, X-ray powder diffraction (XRPD), BET analysis, pore size distribution, and nitrogen adsorption measurements. These characterization results showed that (1) the carboxylate bridged dinuclear rhodium structure was formed with mononuclear copper, nickel, and palladium located at the center of the porphyrin ring were formed in complexes **4**–**6**, and (2) the $[Rh_2(MTCPP)]_n$ possessed numerous uniform micropores (ca. 5.0 Å in diameter) by stacking a 2D lattice structures, and possessed a high nitrogen adsorption capacity. With regard to the hydrogenation of ethene, propene, and 1-butene, (1) complexes **3**–**6** showed high turnover frequencies, and among these and the other reported rhodium-containing materials, it was the most active in complexes **6**, (2) hydrogenation reactions occurred inside the micropores of the complexes **4**–**6**, (3) the activation of hydrogen molecule to from Rh–H species occurred only at the dinuclear rhodium sites, and the metal centers of the porphyrin ring significantly influenced the coordination of olefins, and (4) the activated hydrogen at the bridged dinuclear rhodium sites was transferred to the coordinated olefin molecule onto the metal centers of the porphyrin ring. Catalytic reactions using microporous inorganic–organic hybrid materials, as demonstrated in this paper, would help in obtaining a new strategy for the development of more efficient catalysts.

Acknowledgments

This work was supported by a Grant-in-Aid for Specially Promoted Research, No. 15350088, from the Ministry of Education, Science, Sports and Culture of Japan. This work was also supported by a High-Tech Research Center Project from the Ministry of Education, Culture, Sports, Science and Technology, Japan. CNK is grateful for the support obtained by a Grant-in-Aid for Specially Promoted Research No. 16750126 from the Ministry of Education, Science, Sports and Culture of Japan, and The Association for the Progress of New Chemistry.

References

[1] H. Li, M. Eddaoudi, T.L. Groy, O.M. Yaghi, J. Am. Chem. Soc. 120 (1998) 8571–8572.
[2] W. Mori, F. Inoue, K. Yoshida, H. Nakayama, S. Takamizawa, M. Kishita, Chem. Lett. (1997) 1219–1220.
[3] V.A. Russell, C.C. Evans, W. Li, M.D. Ward, Science (Washington, DC) 276 (1997) 575–579.
[4] M. Kondo, T. Yoshitomi, K. Seki, H. Matsuzaka, S. Kitagawa, Angew. Chem. Int. Ed. Engl. 36 (1997) 1725–1727.
[5] S. Kitagawa, M. Kondo, Bull. Chem. Soc. Jpn. 71 (1998) 1739–1753.
[6] W. Mori, S. Takamizawa, in: A. Nakamura, N. Ueyama, K. Yamaguchi (Eds.), Organometallic Conjugation, Kodansha Springer, Tokyo, 2002, p. 179.
[7] B.F. Hoskins, R. Robson, J. Am. Chem. Soc. 112 (1990) 1546–1554.
[8] E. Lee, J. Kim, J. Heo, D. Whang, K. Kim, Angew. Chem. Int. Ed. 40 (2001) 399–402.
[9] S. Noro, R. Kitaura, M. Kondo, S. Kitagawa, T. Ishii, H. Matsuzaka, M. Yamashita, J. Am. Chem. Soc. 124 (2002) 2568–2583.
[10] O.M. Yaghi, H. Li, T.L. Groy, Inorg. Chem. 36 (1997) 4292–4293.
[11] J.S. Seo, D. Whang, H. Lee, S.I. Jun, J. Oh, Y.J. Jeon, K. Kim, Nature 404 (2000) 982–986.
[12] M. Fujita, Y.J. Kwon, S. Washizu, K. Ogura, J. Am. Chem. Soc. 116 (1994) 1151–1152.
[13] W. Mori, S. Takamizawa, C.N. Kato, T. Ohmura, T. Sato, Micropor. Mesopor. Mater. 73 (2004) 31–46.
[14] C.N. Kato, M. Hasegawa, T. Sato, A. Yoshizawa, T. Inoue, W. Mori, J. Catal. 230 (2005) 226–236.
[15] J.A. Real, E. Andres, M.C. Munoz, M. Julve, T. Granier, A. Bousseksou, F. Varret, Science 268 (1995) 265–267.
[16] S. Naito, T. Tanibe, E. Saito, T. Miyao, W. Mori, Chem. Lett. (2001) 1178–1179.
[17] T. Sato, W. Mori, C.N. Kato, T. Ohnura, T. Sato, K. Yokoyama, S. Takamizawa, S. Naito, Chem. Lett. 32 (2003) 854–855.
[18] T. Sato, W. Mori, C.N. Kato, E. Yanaoka, T. Kuribayashi, R. Ohtera, Y. Shiraishi, J. Catal. 232 (2005) 186–198.
[19] (a) O. Asai, M. Kishita, M. Kubo, Naturwissenschaften 46 (1959) 1–3;
(b) O. Asai, M. Kishita, M. Kubo, J. Phys. Chem. 63 (1959) 96–99.
[20] D. Venkataraman, G.B. Gardner, S. Lee, J.S. Moore, J. Am. Chem. Soc. 117 (1995) 11600–11601.
[21] W. Mori, S. Takamizawa, M. Fujiwara, K. Seki, JP Patent 09132580, 1995 and EP Patent 0727608, 1996.
[22] A. Nakamura, N. Ueyama, K. Yamaguchi (Eds.), Organometallic Conjugation, Kodansha Springer, Tokyo, 2002, p. 179.
[23] (a) W. Mori, H. Hoshino, Y. Nishimoto, S. Takamizawa, Chem. Lett. (1999) 331–332;
(b) R. Nukada, W. Mori, S. Takamizawa, M. Mikuriya, M. Handa, H. Naono, Chem. Lett. (1999) 367–368;
(c) S. Takamizawa, T. Hiroki, E. Nakata, K. Mochizuki, W. Mori, Chem. Lett. (2002) 1208–1209;
(d) S. Takamizawa, E. Nakata, H. Yokoyama, K. Mochizuki, W. Mori, Angew. Chem. Int. Ed. 42 (2003) 4331–4334.
[24] (a) K. Seki, S. Takamizawa, W. Mori, Chem. Lett. (2001) 122–123;
(b) S. Takamizawa, W. Mori, M. Furihata, S. Takeda, K. Yamaguchi, Inorg. Chim. Acta 283 (1998) 268–274;
(c) S. Takamizawa, M. Furihata, S. Takeda, K. Yamaguchi, W. Mori, Macromolecules 33 (2000) 6222–6227.
[25] (a) S. Takamizawa, K. Yamaguchi, W. Mori, Inorg. Chim. Commun. 1 (1998) 177–178;
(b) S. Takamizawa, T. Ohmura, K. Yamaguchi, W. Mori, Mol. Cryst. Liq. Cryst. 342 (2000) 199–204.
[26] (a) K. Seki, S. Takamizawa, W. Mori, Chem. Lett. (2001) 332–333;
(b) K. Seki, Chem. Commun. (2001) 1496–1497.
[27] (a) T. Ohmura, W. Mori, M. Hasegawa, T. Takei, A. Yoshizawa, Chem. Lett. 32 (2003) 34–35;
(b) T. Ohmura, W. Mori, M. Hasegawa, T. Takei, T. Ikeda, E. Hasegawa, Bull. Chem. Soc. Jpn. 76 (2003) 1387–1395.
[28] (a) Z.V. Gryaznova, E.V. Kolodieva, V.P. Paranosenkov, G.V. Tsitsishvili, A.Y. Krupennikova, Neftekhimiya 13 (1973) 374–381;
(b) B.F.G. Johnson, Top. Catal. 24 (2003) 147–159.
[29] (a) J. Hjortkjaer, S. Michael, P. Simonsen, J. Mol. Catal. 6 (1979) 405–420;
(b) E.W. Thornton, H. Knoezinger, B. Tesche, J.J. Rafalko, B.C. Gates, J. Catal. 62 (1980) 117–126;
(c) M.D. Ward, J. Schwartz, J. Mol. Catal. 11 (1981) 397–407;
(d) J.P. Boitiaux, J. Cosyns, E. Robert, Appl. Catal. 35 (1987) 193–209;
(e) F. Sanchez, M. Iglesias, A. Corma, P.C. Del, J. Mol. Catal. 70 (1991) 369–379.
[30] (a) A. Zsigmond, K. Bogar, F. Notheisz, J. Catal. 213 (2003) 103–108;
(b) A. Zsigmond, I. Balatoni, K. Bogar, F. Notheisz, F. Joo, J. Catal. 227 (2004) 428–435.
[31] P.S. Skell, S.N. Ahmed, J. Catal. 125 (1990) 525–540.
[32] H.H. Wagner, H. Hausmann, W.F. Hoelderich, J. Catal. 203 (2001) 150–156.
[33] A.T. Bell, J. Mol. Catal. A 100 (1995) 1–11.
[34] (a) M. Tada, T. Sasaki, Y. Iwasawa, J. Catal. 211 (2002) 496–510;
(b) M. Tada, T. Sasaki, T. Shido, Y. Iwasawa, Phys. Chem. Chem. Phys. 4 (2002) 4561–4574;
(c) M. Tada, Y. Iwasawa, J. Mol. Catal. A 199 (2003) 115–137.
[35] (a) F. Pinna, C. Candilera, G. Strukul, M. Bonivento, J. Org. Chem. 159 (1978) 91–98;
(b) F. Pinna, M. Gonizzi, G. Strukul, G. Cooco, S. Enzo, J. Catal. 82 (1983) 171–176.
[36] (a) I. Feinstein-Jaffe, A. Efraty, J. Mol. Catal. 35 (1986) 285–302;
(b) I. Feinstein-Jaffe, A. Efraty, J. Mol. Catal. 40 (1987) 1–7.
[37] F.R. Hartley (Ed.), Chemistry of the Platinum Group Metals: Recent Development, Elsevier Science, New York, 1991.
[38] K.J. Williams, M.E. Levin, M. Salmeron, A.T. Bell, G.A. Somorjai, Catal. Lett. 1 (1988) 331–338.
[39] S. Naito, M. Tanimoto, J. Catal. 102 (1986) 377–385.
[40] S. Naito, K. Oguni, T. Naito, T. Miyao, Stud. Surf. Sci. Catal. 130 (2000) 2351–2356.
[41] (a) J.M. Thomas, R. Raja, Chem. Rec. 1 (2001) 448–466;
(b) A. Frydman, D.G. Castner, C.T. Campbell, M. Schmal, J. Catal. 188 (1999) 1–13;
(c) T. Yokoyama, K. Yamazaki, N. Kosugi, H. Kuroda, M. Ichikawa, T. Fukushima, J. Chem. Soc., Chem. Commun. (1984) 962–963;
(d) M. Ichikawa, Polyhedron 7 (1988) 2351–2367;
(e) A. Choplin, L. Huang, A. Theolier, P. Gallezot, J.M. Basset, U. Siriwardane, S.G. Shore, R. Mathieu, J. Am. Chem. Soc. 108 (1986) 4224–4225.
[42] J.R. Anderson, D.E. Mainwaring, J. Catal. 35 (1974) 162–165.
[43] L. Tebassi, A. Sayari, A. Ghorbel, M. Dufaux, C. Naccache, J. Mol. Catal. 25 (1984) 397–408.
[44] Y. Huang, W.M.H. Sachtler, J. Catal. 188 (1999) 215–225.
[45] G.D. Angel, B. Coq, F. Figueras, J. Catal. 95 (1985) 167–180.
[46] J.R. Budge, B.F. Lucke, B.C. Gates, J. Toran, J. Catal. 91 (1985) 272–282.
[47] V. Schunemann, H. Trevino, G.D. Lei, D.C. Tomczak, W.M.H. Sachtler, K. Fogash, J.A. Dumesic, J. Catal. 153 (1995) 144–157.

[48] S. Irusta, L.M. Cornaglia, E.A. Lombardo, J. Catal. 210 (2002) 263–272.
[49] (a) K.I. Choi, M.A. Vannice, J. Catal. 131 (1991) 22–35;
(b) K.I. Choi, M.A. Vannice, J. Catal. 131 (1991) 36–50.
[50] K. Nakano, K. Kusunoki, Chem. Eng. Commun. 34 (1985) 99–109.
[51] R.J. Pellet, J. Catal. 177 (1998) 40–52.
[52] (a) A. Zhang, I. Nakamura, K. Fujimoto, J. Catal. 168 (1997) 328–333;
(b) E. Baumgarten, R. Krupp, React. Kinet. Catal. Lett. 70 (2000) 27–33;
(c) M. Ojeda, G.M. Lopez, S. Rojas, P. Terreros, J.L.G. Fierro, J. Mol. Catal. A 202 (2003) 179–186.
[53] (a) J.A. Osborn, F.H. Jardine, J.F. Young, G. Wilkinson, J. Chem. Soc. A (1966) 1711–1732;
(b) F.H. Jardine, J.A. Osborn, G. Wilkinson, J. Chem. Soc. A (1967) 1574–1578;
(c) J. Halpern, T. Okamoto, Inorg. Chem. Acta 89 (1984) L53–L54;
(d) Y. Ohtani, A. Yamagishi, M. Fujimoto, Bull. Chem. Soc. Jpn. 52 (1979) 69–72.